Spring 2013

Transmission shaft design for hydrokinetic turbine with reliability consideration

Goutham Pusapati

Department:

TRANSMISSION SHAFT DESIGN FOR HYDROKINETIC TURBINE WITH RELIABILITY CONSIDERATION

by

GOUTHAM PUSAPATI

A THESIS

Presented to the Faculty of the Graduate School of the

MISSOURI UNIVERSITY OF SCIENCE AND TECHNOLOGY

In Partial Fulfillment of the Requirements for the Degree

MASTER OF SCIENCE IN MECHANICAL ENGINEERING

2013

Approved by

Dr. Xiaoping Du, Advisor
Dr. Ashok Midha
Dr. Serhat Hosder

ABSTRACT

Hydrokinetic energy, a relatively new kind of renewable energy, can be generated from flowing water in rivers or oceans. Hydrokinetic turbines (HKTs) are a major system for hydrokinetic energy, and the reliability of the HKTs is critical for both their lifecycle cost and safety. The objective of this work is to apply advanced methodologies of reliability analysis and reliability-based design to the transmission shaft design for a horizontal-axis, non-submerged HKT. The deterministic shaft design is performed first by considering failure modes of strength and deflection using distortion energy, maximum shear and deflection theories. Then the reliability analysis of the shaft designed is performed by using Sampling Approach to Extreme Values of Stochastic Process method (SAEVSP). Finally reliability-based design is applied to the transmission shaft design, which results in the minimal shaft diameter that satisfies the reliability requirement for a given period of operation time. Since the time-dependent river velocity process is involved, the time-dependent reliability method is used in the reliability-based design. The methodology for the shaft design in this work can be extended to the design of other components in the HKT system.

ACKNOWLEDGMENTS

I would like to express my sincere gratitude to my advisor, Dr. Xiaoping Du for all his support and motivation throughout my master's program at Missouri University of Science and Technology. He was always welcoming and was very patient in helping me overcome many crisis situations and finish this thesis. He is a gifted teacher and an amazing person. One simply could not wish for a better advisor.

It gives me great pleasure in acknowledging my committee members Dr. Ashok Midha and Dr. Serhat Hosder for agreeing to be on my thesis committee despite their extremely busy schedule. I would also like to thank Ms. Katherine Wagner for her patience in answering all of my enquiries at various stages during my program. I also wish to thank Ms. Elizabeth Roberson and Ms. Erin Rowe of Office of Graduate studies for reviewing my thesis.

This thesis would not have been possible without the help and support from my research mate and friend, Zhen Hu. His willingness to help and his good nature has been an inspiration to me in becoming a better person both in my academic and personal life.

Finally, I am most grateful to my parent, grandparents and my sister Geetha Buddharaju for their continuous support and encouragement in my educational endeavors and for always being there for me.

TABLE OF CONTENTS

LIST OF ILLUSTRATIONS

LIST OF TABLES

1. INTRODUCTION

Particle pollution from power plants is estimated to kill approximately 13,000 people a year [1]. This statement demonstrates the level of need for an alternative source of energy for the present world we live in. As long as fossil fuels remain dominant sources of energy we will not be able to stop the ever-growing pollution that is happening nearly everywhere in our planet. Renewable energy is the key in stopping environmental pollution.

Hydrokinetic Energy is a relatively new field of renewable energy. Not much work has been done in design of hydrokinetic turbines. This thesis presents the design model for a transmission shaft of a horizontal axis hydrokinetic turbine with a non-submerged generator. A traditional design approach and probabilistic design approach are followed for the transmission shaft design and compared.

1.1. RESEARCH OBJECTIVE

The objective of this study is to design a transmission shaft for a proposed horizontal axis hydrokinetic turbine. This is to be done by analyzing the failure modes of the transmission shaft and their effects on reliability of the system. This is accomplished by first designing the transmission shaft for all the possible failure modes using traditional design procedure. The failure modes are considered for reliability analysis with a conservative attitude. Based on the results from reliability analysis, a reliability-based design optimization of the shaft is performed and the results are discussed.

Since precise data for the configuration of the hydrokinetic turbine are unavailable, the total procedure is based on a conceptual specification for a hydrokinetic turbine. This model can be later applied for a specific configuration for a similar design

problem in future. A conceptual illustration of the hydrokinetic turbine blade and transmission shaft assembly is shown in Figure 1.1.

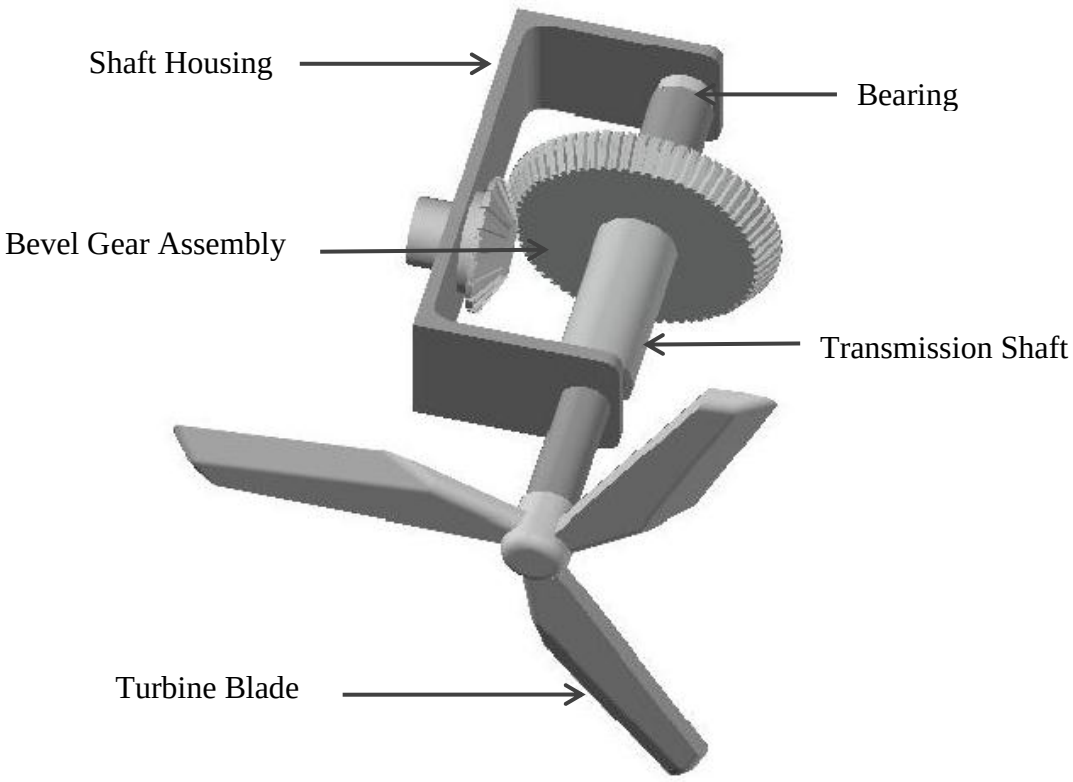

Figure 1.1. Hydrokinetic turbine shaft assembly

1.2. HYDROKINETIC ENERGY

Conventional hydropower plants have been major contributors to renewable energy. Presently, the hydropower facilities in the U.S. can generate enough hydropower to supply electricity to 28 million households, which is equivalent to about 500 million barrels of oil [2]. But, the growth of conventional hydropower plants is restricted by the limited number of available natural sites, huge initial investment, environmental and

ecological concerns. Marine and hydrokinetic turbines on the other hand offer many advantages compared to hydropower plants. They are portable systems with relatively small initial cost, lesser infrastructure and are easy to deployment [3] [4] [5] [6]. The US rivers hydrokinetic power potential is estimated to be 12,500 MW from study conducted by New York University [7]. This estimate shows the potential and prospect for hydrokinetic systems.

Hydrokinetic energy can be described as the energy that can be generated from flowing water that occurs in rivers or ocean currents. This includes ocean wave energy, tidal energy, river in-stream energy, and ocean current energy. As of today, there are not many hydrokinetic energy projects in commercial operation. However, there are several proposed wave energy projects worldwide, and a number of operating prototype systems under testing. River in-stream generating facilities are in the development stage with several operating prototypes being tested. Regardless of this comparatively low level of development, hydrokinetic energy resource has a significant potential, and it is a renewable resource which does not produce greenhouse gas and thus environmentally safe.

This procedure of power generation in hydrokinetic energy is similar to that of wind turbines where wind is the fluid medium. Hydrokinetic turbines differ from conventional hydroelectric turbines for the same. The rotor of the Hydrokinetic turbine is immersed in the flowing water and the kinetic energy of the water is used to rotate the rotor blades which are coupled to a generator which produces power. The hydrokinetic turbines are also called as zero-head turbines as they do not need water head for operation unlike hydroelectric turbines.

A typical hydrokinetic energy system is shown in Figure 1.2. For the hydrokinetic energy system described in Figure 1.2, the blades of the turbine rotate from the flow of the water. The torque generated at the rotor in then sent to the generator using the power transmission. The speed is adjusted according to the generator at the gear box. Now the mechanical energy is converted into electricity at the generator. This electricity generated is now altered and sent to the power grid using a control system.

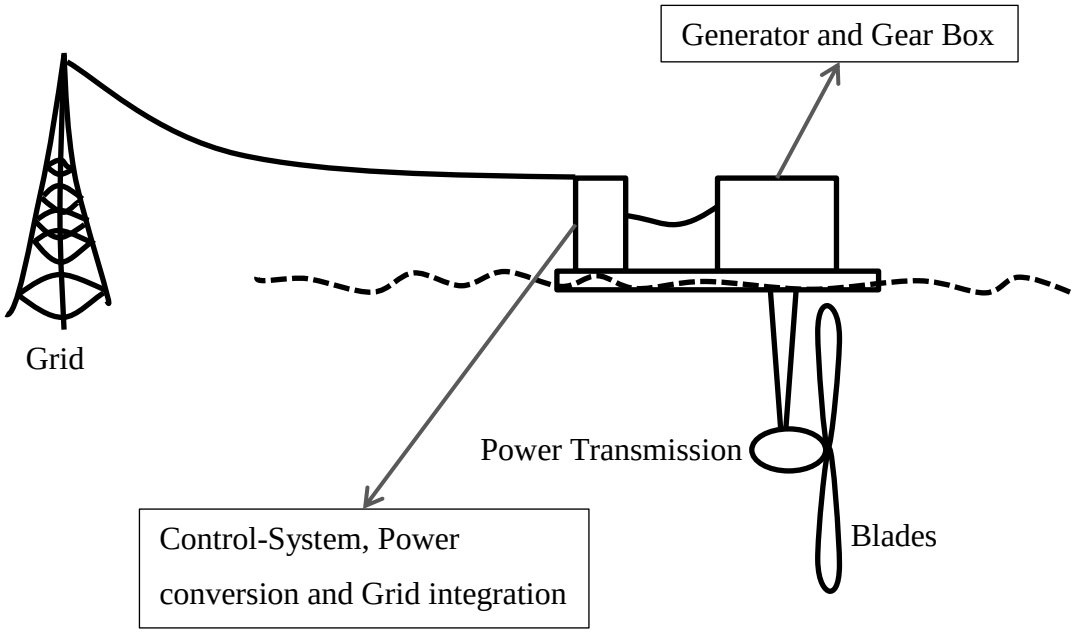

Figure 1.2. Outline of a hydrokinetic energy system [10]

1.3. THESIS OUTLINE

The succeeding section is a literature review of introduction to hydrokinetic turbines, uncertainty in design, reliability analysis and reliability-based design. Different types of hydrokinetic turbine specifications are discussed. In the uncertainty in design section, a short introduction related to uncertainty in design and various uncertainties

involved in design are presented. This is followed by a review of the reliability analysis and reliability-based design from a mechanical design perspective.

Section 3 consists of the deterministic/traditional design methodology. This chapter starts with analyzing the forces acting on the transmission shaft under consideration. This is used to determine the possible failure modes for the shaft. Now a sample hydrokinetic turbine configuration is discussed and is used to determining the minimum diameter for the transmission shaft.

Section 4 contains the reliability analysis procedure used to determine the reliability of the traditional design. The velocity of the water is considered as a time variant uncertainty for the analysis. Then a reliability-based design optimization is performed accommodate the uncertainties that are ignored by the traditional design.

Section 5 includes drawing conclusions from the above analysis. It contains the discussion on the design methodologies and conclusions taken from the findings. A brief insight of future work on the topic is proposed. A flowchart of the outline is presented in Figure 1.3.

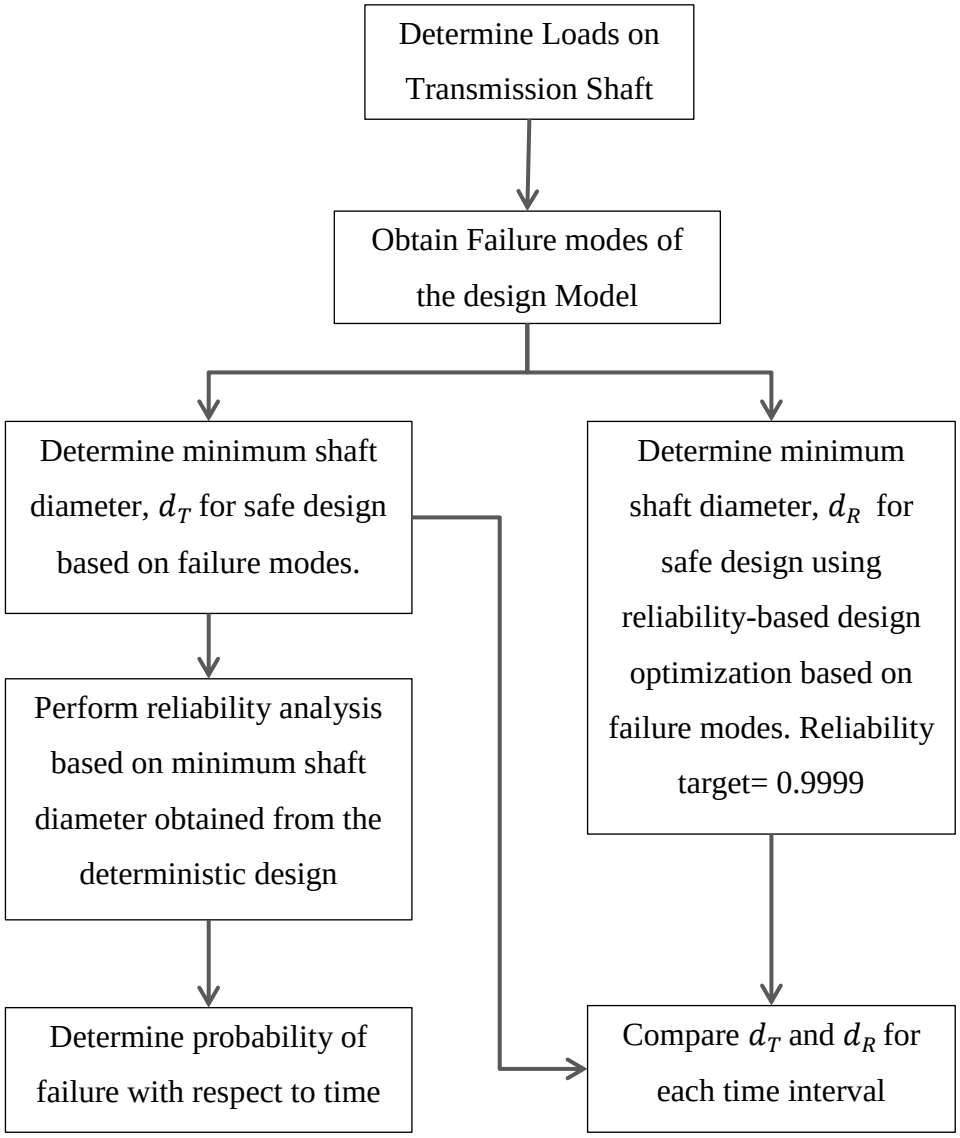

Figure 1.3. Flow chart of thesis outline

2. LITERATURE REVIEW

2.1. HYDROKINETIC TURBINES

The rotor of the hydrokinetic turbine is similar to that of the wind turbine generating power from converting the energy from flow of fluid (water in case of hydrokinetic turbine) into rotational power. The shape, angle of deflection, and spacing of blades can play a major role in the efficiency of a turbine and is the main area of research in developing the best hydrokinetic turbine suited for a specific application. The hydrokinetic turbines are also known as zero head turbines because they do not need water head for their operation and convert flowing water into mechanical work [8] [9]. The design and technology for hydrokinetic turbines is often adapted from that of the wind turbines because of these understandable similarities they share.

The hydrokinetic turbines are classified based on the alignment of the shaft [10]. They are broadly classified as horizontal axis, vertical axis and cross flow turbines. Horizontal and vertical axis turbines are most widely used. The choice of selection depends on various technical factors at the installation site and other financial aspects.

2.1.1. Horizontal Axis Turbine. The shaft is aligned in a direction parallel to the direction of flow of water in a horizontal axis turbine. Hence they are also called as axial flow turbines. The generator is usually placed above the water level. The generator and the rotor blades are connected by a bevel gear or a belt drive or other power transmission means depending on the site conditions.

The turbine may be mounted in numerous ways as shown in the Figure 2.1. The turbines with rigid mooring are placed on riverbeds and seafloors [10]. Then a floating

mooring mechanism is used depending on the site conditions. In case of rivers, the velocity of water is usually high at the surface compared to that at the river bed with makes its ideal to consider a floating mooring system.

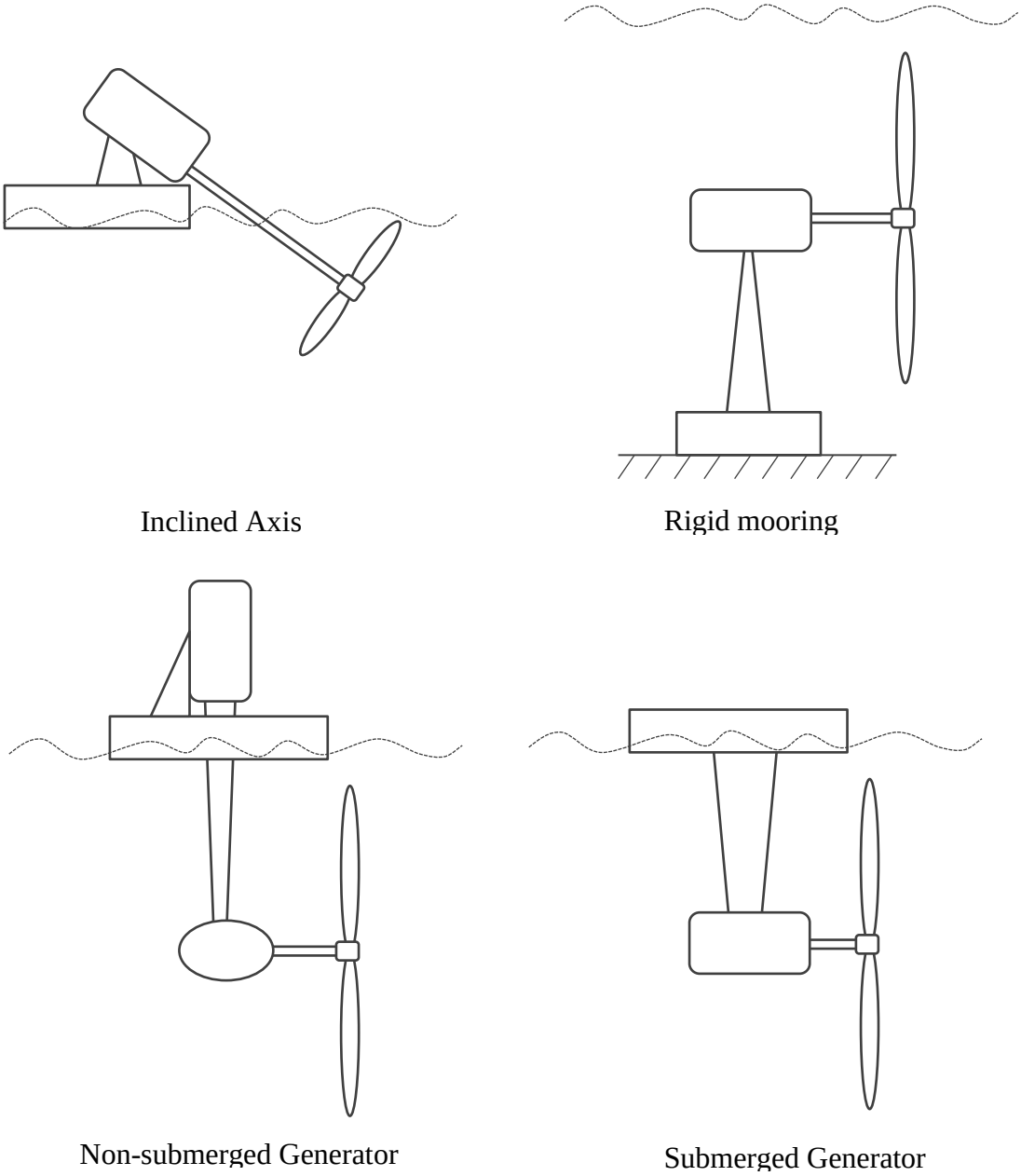

Figure 2.1. Types of horizontal axis turbines [10]

2.1.2. Vertical Axis Turbine. The vertical axis turbines, in contrary to horizontal axis turbines have their axis perpendicular to the direction of flow of water. They usually have uniform cross-section blades fixed to two flat plates at the top and bottom [10]. A number of blades are fixed in a way to maximize the power generated from the water flow. Figure 2.2 shows the various configurations of vertical axis turbines.

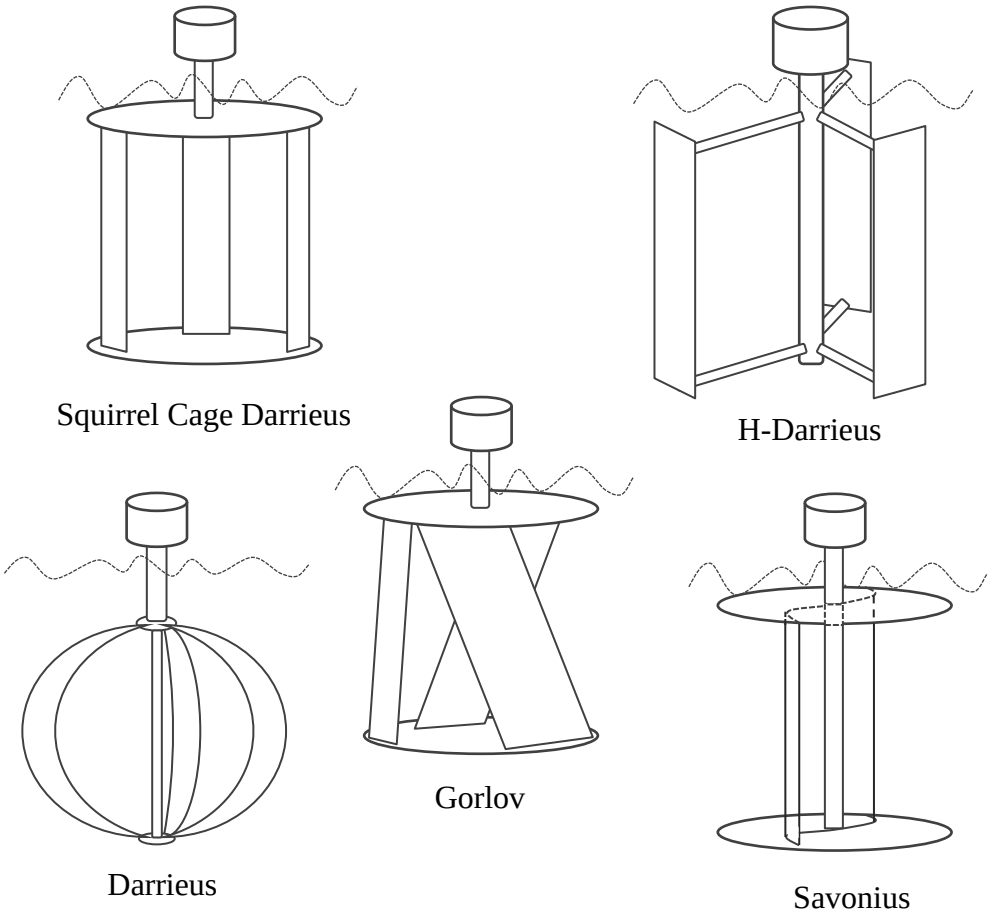

Figure 2.2. Types of vertical axis turbines [10]

2.1.3. Transmission Shaft. The transmission shaft in a hydrokinetic turbine is the first component to receive the power generated at the turbine blade. The role of the transmission shaft in the hydrokinetic turbine system is to transmit the torque generated at the turbine blades to the generator. This is done using mechanical power transmission components such as chain, gears, sprockets, belts, pulleys, universal joints, clutches mounted on the transmission shaft. The shaft as a result is subjected to a variety of loading. In design of the shaft therefore it is necessary to account for all the loading on the shaft.

The uncertainties involved in the design process of a transmission shaft include uncertainty in loading conditions, modeling uncertainties and physical uncertainties. It is necessary to take into consideration all these uncertainties to design a reliable shaft.

Reliability is a key requirement for consistently delivering acceptable system performance for a given time period. Reliability of the hydrokinetic system as a whole is dependent on individual component reliability. Failure of transmission shaft in a hydrokinetic turbine will result in the failure of the system as a whole. Hence reliability of the transmission shaft is vital for the hydrokinetic turbine.

2.2. UNCERTAINTIES IN DESIGN

While designing a component or a system as a whole, it is vital to take into consideration the uncertainties involved in the design parameters and design models. From a design point of view, uncertainties can be classified into the following:

2.2.1. Physical Uncertainties. These uncertainties are also denoted as aleatory uncertainties. Uncertainties involving the natural randomness in various physical parameters such as the annual maximum river flow velocity and material properties.

2.2.2. Model Uncertainties. Model uncertainties as the name suggests is the uncertainty associated with the design model, often because of the approximations and other factors involved in it. It also includes the uncertainty associated with modeling the distribution functions of the involving random variables in the design process.

Statistical uncertainties are a type of model uncertainty. They correspond to the uncertainty caused from limiting number of data available to determine the statistical characteristics of a parameter.

2.2.3. Measurement Uncertainties. Measurement uncertainty is related to the uncertainty related to imperfection cased in measurement of a physical parameter.

Model uncertainties, statistical uncertainties and measurement uncertainties are denoted as epistemic uncertainties. This is because these uncertainties are caused due to lack of knowledge.

2.3. RELIABILITY ANALYSIS AND RELIABILITY-BASED DESIGN

2.3.1. Reliability. Reliability by definition is "the ability of a system or component to perform its required functions under stated conditions for a specified period of time [11]". In simple probabilistic terms, it is the probability that a system or component does not fail in a given set of conditions. Hence a system or component with a high reliability corresponds to low chances of failure and thus is a better designed product. Mathematically reliability is computed as follows:

$$R = 1 - P_f = P\{g(\boldsymbol{X}) > 0\} \tag{2.1}$$

and probability of failure is defined as:

$$P_f = P\{g(\boldsymbol{X}) < 0\} \tag{2.2}$$

where $\boldsymbol{X}$ is the vector of random variables $\boldsymbol{X} = (X_1, X_2, \dots, X_n)$, and the condition for safety is defined as $g(\boldsymbol{X}) > 0$. Noticeably the region of failure is defined as $g(\boldsymbol{X}) < 0$. The function $g(\boldsymbol{X})$ is called the Limit-state function that defines the state of the system.

$$g(X_1, X_2, \dots, X_n)\begin{cases} > 0 & \text{Safe state} \\ = 0 & \text{Limit state} \\ < 0 & \text{Failure state} \end{cases} \tag{2.3}$$

2.3.2. Reliability Analysis. The Limit-state functions acts as a border to determine and separated safe region and failure region. Consider a performance function of two random variables $\boldsymbol{X_1}$ **and** $\boldsymbol{X_2}$ given by g $(\boldsymbol{X_1}, \boldsymbol{X_2})$. An illustration of the design space is shown in Figure 2.3. Consider that the reliability of the system is .99. This means that 99% of the actual design points lie within the safe region. It is vital in design to determine the probability that the response of a design is in the safe region. Thus the performance function plays an important role in the assessment of reliability of a design.

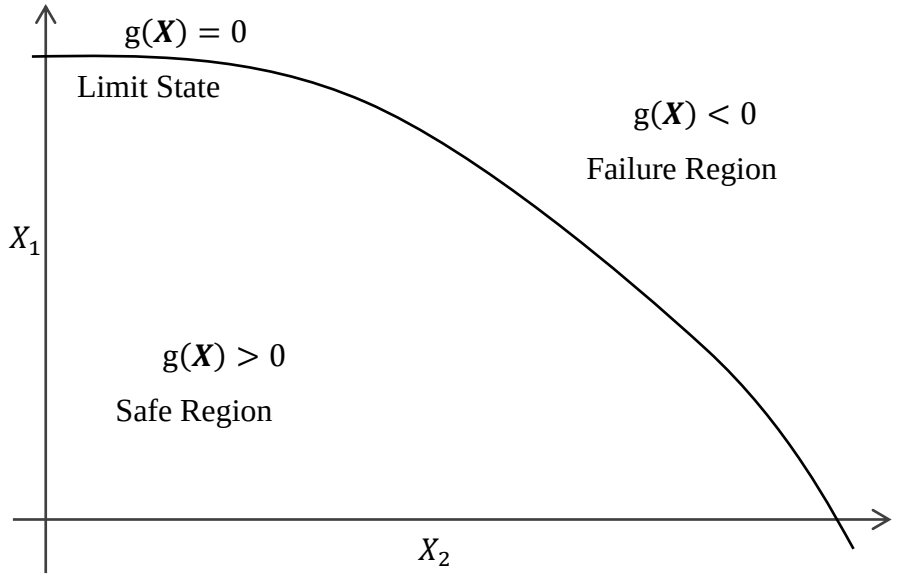

Figure 2.3. Design Space

In the figure, the limit-state function for a two dimensional plane(X_1, X_2), $g(\boldsymbol{X}) = 0$, separates the safe design space $g(\boldsymbol{X}) > 0$ from the failure space $g(\boldsymbol{X}) < 0$. Reliability is now computed as the area of the joint probability density function (PDF) of X_1 and X_2 lying in the safe design region $g(\boldsymbol{X}) > 0$. Because of the uncertainties present in the random variables (X_1, X_2), the limit-state function is a random variable by itself.

Reliability Analysis is the methodology used to determine the probability that the limit-state function for a given set of random variables belong to the safe region. In simple terms it is determining the reliability given in Equation 2.1. Reliability is determined based on failure modes of the component or system. Typical failure modes include, exceeding of ultimate strength, local and global instability/buckling and

exceeding acceptable deflection. Limit-state functions from reliability analysis standpoint can be classified depending on input random variables as follows:

$$Z = g_1(\boldsymbol{X}, t) \tag{2.4}$$

where $g_1(.)$ is the limit-state function involving time invariant random variables $\boldsymbol{X}$ and time t. Z is the response variable.

$$Z = g_2(\boldsymbol{X}, \boldsymbol{Y}(t)) \tag{2.5}$$

where $g_2(.)$ is the limit-state function involving time invariant random variables $\boldsymbol{X}$ and time dependent random variables $\boldsymbol{Y}$ (stochastic process).

$$Z = g_3(\boldsymbol{X}, \boldsymbol{Y}(t), t) \tag{2.6}$$

where $g_3(.)$ is the limit-state function involving time invariant random variables $\boldsymbol{X}$, time dependent random variables $\boldsymbol{Y}$ and time t.

Many progresses have been made in reliability analysis methodologies. They vary in accuracies, efficiency and application in terms of limit-state function used. Some of the popular ones include Monte Carlo Simulation (MCS) [12], First and Second Order Reliability Method (FORM and SORM) etc. MCS and FORM are used for the reliability analysis in this thesis. They are described in detail in chapter 4.

2.3.3. Reliability-Based Design (RBD). RBD is a design approach where the reliability of the component or system being designed is considered as a design constraint [13]. This is done taking into consideration uncertainties of the random variables involved in the design process. Thus this methodology is more practical and is real world oriented compared to traditional design methodologies. This ensures safer design solution.

Reliability Based Design Optimization (RBDO) is an optimization process where the objective is a cost-type function [14] [15] [16]. For example for optimizing the cross-sectional area of a column for a given constraint set, the objective would be to minimize the cross-section. The constraint equations in the optimization model in RBD optimization include the reliability constrain in particular and other design constraints [17] [18]. The reliability constraint is defined as the probability that the response of the limit-state function lies in the safe design:

$$R \leq P\{g(\boldsymbol{X}) > 0\} \tag{2.7}$$

where R is the reliability and $g(\boldsymbol{X}) > 0$, is defined as the safe design region.

3. DETERMINISTIC TURBINE SHAFT DESIGN

3.1. INTRODUCTION

Deterministic component design is traditional mechanical design, where uncertainties of the variables involved in the design are not accounted for [19]. For instance, loads in a deterministic design are considered unchanging. This is not the case in real life. Probabilistic design is an iteration of deterministic design where the randomness of the variables is incorporated in the design.

In this chapter the overall deterministic shaft design process is presented. The main objective in our case is to determine the minimum diameter of a transmission shaft to transmit power generated from the water flow at the turbine blades to the generator. A bevel gear is to be mounted on the shaft to redirect torque generated from the horizontally mounted turbine blade to the vertical generator input shaft. The transmission shaft is mounted on inverted U shaped casing with bearing mounts.

The list below outlines the shaft design procedure followed.

1. Determine external loads and forces acting on the shaft.
2. Choose preliminary shaft configuration.
3. Select a material for the shaft
4. Produce shear force and bending moment diagrams and determine shear and direct stress.
5. Perform stress and deflection analysis.
6. Specify shaft diameter.
7. Predict shaft life based on fatigue.

3.2. DETERMINE EXTERNAL LOADS AND FORCES ACTING ON THE SHAFT

The torque and thrust at the blades are the major external forces acting on the system and therefore are considered as the primary forces acting on the transmission shaft. The thrust does not lead to any bending moment because the horizontal component of thrust (acting parallel to the axis of the shaft) cancel each other due to the symmetry and accounts to only a normal force along the axis of the shaft. The bevel gear assembly mounted on the transmission shaft exerts secondary forces (force perpendicular to the axis of shaft) and a bending-moment on the shaft.

3.2.1. Torque and Thrust on the Blade (primary forces). Torque and thrust on the blades is determined using the Bade Element Momentum (BEM) theory. Though more sophisticated methods are available, this method has the advantage being simple and effective.

BEM Theory equates two methods of examining turbine operation. The first method is to use a momentum balance on rotating annular stream tube passing through the turbine. The second method is examining aerofoil lift and drag coefficients at various sections along the blade. The equations derived from the two methods are then solved iteratively. The key assumptions in the theory are that there are no aerodynamic interactions between different blades and that the forces are solely determined by lift and drag coefficients.

3.2.1.1 Method 1: Momentum Balance. The following discussions in the BEM theory are presented with a thought that the reader has background of fluid dynamics and 1-D momentum theory [20].

Figure 3.1 illustrates a stream tube and the control volume considered for the BEM theory. The flow across the blades (stream tube) is discretized into N annular elements of height dr and these elements are laterally streamlined (no slow across elements). The force from the blades on the flow is considered consistent in each of the annular element (assuming a rotor of infinite blades).This assumption is rectified using Prandtl's tip correction factor in order to compute for a finite number of blades. The thrust from an annular element on the control volume is determined using integral momentum equation.

The thrust is given by:

$$dF_T = (V_0 - u_1)d\dot{m}. \tag{3.1}$$

V_0 is the water speed far upstream, u_1 is speed at wake and $d\dot{m}$ is the flow rate.

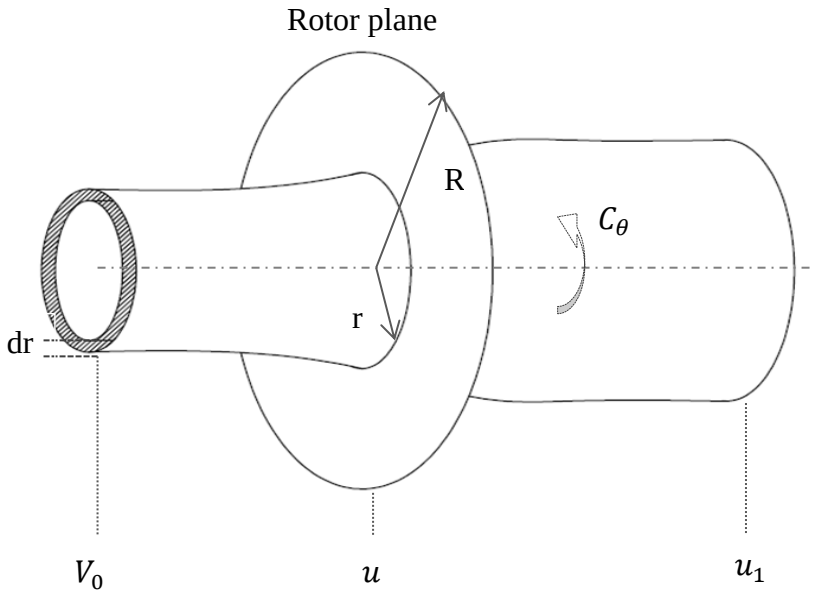

Figure 3.1. Control volume around wind turbine [20]

The flow rate is $d\dot{m} = 2\pi r\rho u dr$, where r is the radius of the annular element, ρ is the density of water and u is water speed at the rotor plane. Thus Equation (3.1) can be written as

$$dF_T = 2\pi r\rho u(V_0 - u_1)dr. \tag{3.2}$$

The toque is determined using the integral moment of momentum, setting the rotational velocity to zero upstream and C_θ in the wake. The torque is given by:

$$dT = rC_\theta d\dot{m} = 2\pi\rho r^2 u C_\theta dr. \tag{3.3}$$

where C_θ is rotational velocity in the wake.

The axial velocities u and u_1 can expressed in terms of the water velocity V_0 using axial induction factor a as

$$u = (1 - a)V_0. \tag{3.4}$$

$$u_1 = (1 - 2a)V_0. \tag{3.5}$$

Similarly the rotational velocity in the wake C_θ can be expressed in terms of angular velocity of the blade ω using a' as

$$C_\theta = 2a'\omega r. \tag{3.6}$$

where a' is the rotational induction factor.

Introducing Equations (3.4), (3.5) and (3.6) and Prandtl's tip loss factor F into Equations (3.2) and (3.3), the thrust and torque can be computed as:

$$dF_T = 4\pi r\rho V_0^2 a(1-a)Fdr. \tag{3.7}$$

$$dT = 4\pi\rho r^3 V_0\omega(1-a)a'Fdr. \tag{3.8}$$

where

$$F = \frac{2}{\pi}\cos^{-1} e^{-f} \tag{3.9}$$

$$f = \frac{B}{2}\frac{R-r}{r\sin\varphi} \tag{3.10}$$

and B is the number of blades, R is the total radius of rotor, r is the local radius and φ is the flow angle.

3.2.1.2 Method 2: Aerofoil lift and drag. From 2-D aerodynamics, the lift and drag are defined as forces perpendicular and parallel to the relative velocity $\boldsymbol{V_{rel}}$ at the aerofoil respectively. Given that lift and drag coefficients $\boldsymbol{C_l}$ and $\boldsymbol{C_d}$ and the chord length $\boldsymbol{c}$ are known for a particular aerofoil, the lift and drag forces per unit length can be determined from Equations (3.11) and (3.12).

$$L = \frac{1}{2}\rho V_{rel}^2 c C_l \tag{3.11}$$

$$D = \frac{1}{2}\rho V_{rel}^2 c C_d \tag{3.12}$$

where L is the lift and D is the drag.

The normal force p_N and tangential force p_T per unit length in the rotational plane of the blades can be deduced from lift and drag as

$$p_N = L\cos\varphi + D\sin\varphi. \tag{3.13}$$

$$p_T = L\sin\varphi - D\cos\varphi. \tag{3.14}$$

where p_N is the normal force, p_T is the tangential force, φ is the flow angle; the angle between plane of rotation and the relative velocity. The lift and drag coefficients C_l and C_d are determined based on local angle of attack α given by $\alpha = \varphi - \theta$. Here θ is the local pitch as shown in Figure 3.2.

Considering $C_n = C_l\cos\varphi + C_d\sin\varphi$ and $C_t = C_l\sin\varphi - C_d\cos\varphi$ and rewriting Equations (3.13) and (3.14) yield

$$p_N = \frac{1}{2}\rho V_{rel}^2 c C_n \tag{3.15}$$

$$p_T = \frac{1}{2}\rho V_{rel}^2 c C_t \tag{3.16}$$

where c is the chord length.

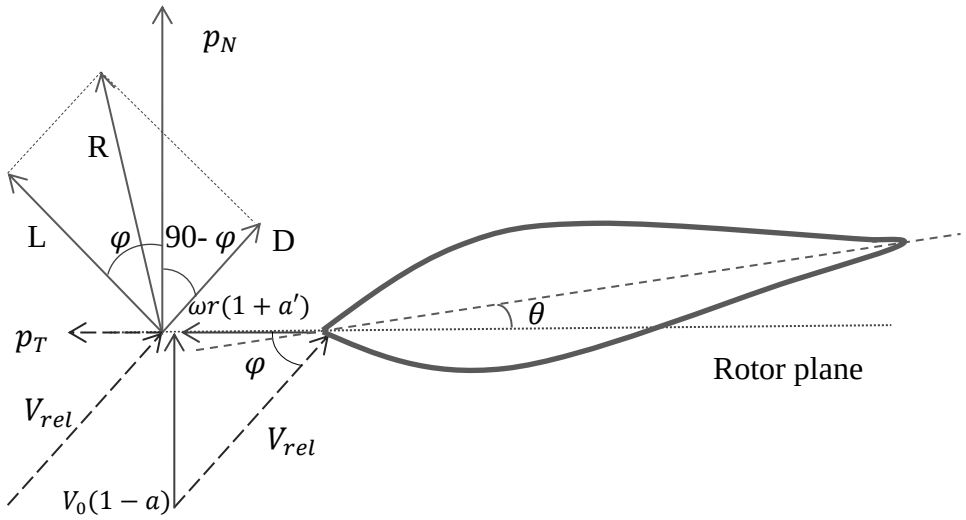

Figure 3.2. Velocities at rotor plane [20]

From the geometry of the aerofoil (Figure 3-2), a relation between the relative velocity V_{rel} , water velocity V_0, and angular velocity of the blades ω can be established as

$$V_{rel}\sin\varphi = V_0(1-a) \tag{3.17}$$

$$V_{rel}\cos\varphi = \omega r(1+a') \tag{3.18}$$

From the forces per unit length p_N and p_T, the thrust and torque on the control volume of thickness dr are

$$dF_T = Bp_N dr \tag{3.19}$$

$$dT = rBp_T dr \tag{3.20}$$

where B is the number of blades.

Using Equation (3.15) for p_N and equation (3.17) for V_{rel}, Equation (3.19) can be rewritten as

$$dF_T = \frac{1}{2}\rho B \frac{V_0^2(1-a^2)}{sin^2\varphi} cC_n dr \tag{3.21}$$

Similarly, using Equation (3.16) for p_N and Equation (3.18) for V_{rel}, Equation (3.20) can be rewritten as

$$dT = \frac{1}{2}\rho B \frac{V_0(1-a)\omega r(1+a')}{\sin\varphi\cos\varphi} cC_t r dr \tag{3.22}$$

An expression for the axial induction factor a can be obtained from equating Equations (3.21) and (3.2) for dF_T

$$a = \frac{1}{\frac{4Fsin^2\varphi}{\sigma C_n}+1} \tag{3.23}$$

where σ is solididty defined as $\sigma(r) = \frac{c(r)B}{2\pi r}$, $\frac{c(r)B}{2\pi r}$ is fraction of annular area in control volume covered by blades.

Similarly, an expression for a' can be obtained from equating Equations (3.22) and (3.3) for dT and using Equation (3.23)

$$a' = \frac{1}{\frac{4F\sin\varphi\cos\varphi}{\sigma C_t}-1} \tag{3.24}$$

Equations for thrust (3.21) and torque (3.22) for each annular element are now derived and can be used to determine total thrust and torque by integrating over the control volume. Now the total thrust and torque are the primary forces acting on the shaft and can be used to determine secondary forces.

3.2.2. Forces Exerted from Bevel Gear Assembly (Secondary Forces). A straight bevel gear is used to transmit the torque from the blades to a generator with its axis mounted perpendicular to the axis of the turbine blades. A straight or spiral bevel gear could be used to transmit torque in the perpendicular axis, but a straight bevel gear has the advantage of being applicable for higher torque and speed transmission and hence is considered feasible for the application.

In determining shaft and bearing loads for the bevel gear application, the usual practice is to use tangential or transmitted load that would occur if all the forces were concentrated at the midpoint of the tooth. The actual resultant occurs somewhere between the mid-point and large end of the tooth, but is only an insignificant error in making this assumption. The transmitted load W_t is given by

$$W_t = \frac{T}{r_a} \tag{3.25}$$

where T is the torque transmitted and r_a is the pitch radius at the mid-point of the gear tooth.

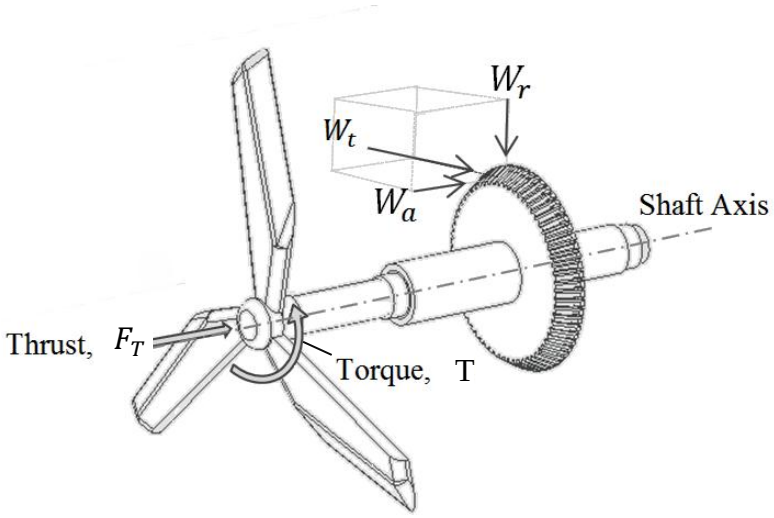

Figure 3.3. Forces action on transmission shaft

W_r and W_a are the perpendicular components of the resultant forces, perpendicular and parallel to the axis of the transmission shaft respectively. From the trigonometry of the loading at the gear, W_r and W_a are given by

$$W_r = W_t \tan\theta \cos\gamma \tag{3.26}$$

$$W_a = W_t \tan\theta \sin\gamma \tag{3.27}$$

where $\theta$and γ are pressure angle and pitch angle for the gear system respectively. The pitch angle γ is defined as $\tan\gamma = \frac{N_P}{N_G}$, where N_P and N_G are the tooth numbers for pinion and gear respectively.

3.3. CHOOSE PRELIMINARY SHAFT CONFIGURATION

Shaft geometry is usually similar to that of a stepped cylinder. The use of shoulders is an excellent means of axially locating the shaft elements. Shoulders can also be used to preload rolling bearings and to provide necessary thrust reactions to the rotating elements.

The geometric configuration of the transmission shaft is mostly taken from existing shafts used for similar applications. An example for an application is shown in Figure 3-4, where a bevel gear is used in a similar assembly.

Figure 3.4. Example of a similar application

For our case, provision has to be given for bearings and the bevel gear assembly. A plan for the shaft configuration is prepared using elements from existing configurations. Figure 3-5 gives an illustration of the design model. The bearings at section A and D are preloaded with inner rings press-fitted to the shaft. Since shoulders are designed to take thrust loads, a tapered roller bearing need or need not be used to counter the thrust loads. A torque transmitting element is required in order to transmit torque from the shaft to the bevel gear. Though there are many torque transfer elements like splines, setscrews, pins tapered fits etc., for this keys or pins are ideal because of their ability to take torsional and thrust loads. For the model a key is considered for the analysis because keys have higher axial load handling capacity. Section B is used to axially place bevel gear. Turbine blade is mounted at section E.

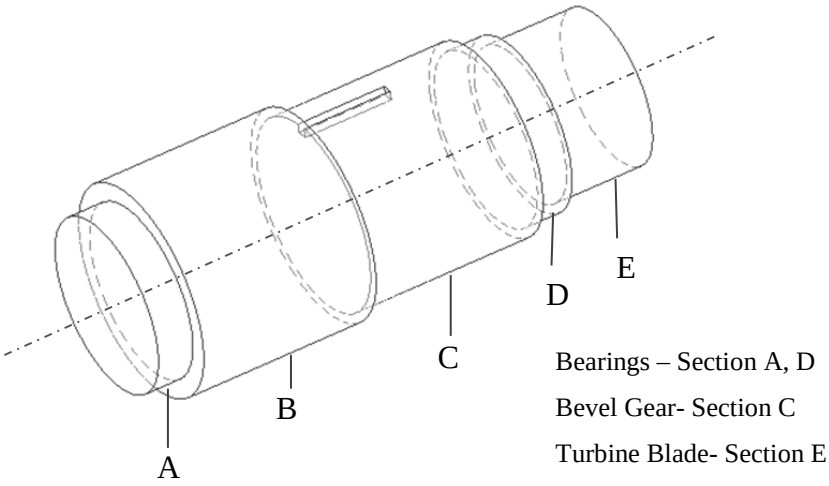

Figure 3.5. Different sections of the transmission shaft

3.4. SELECT A MATERIAL FOR THE SHAFT

Material selection is an important segement of the design process which plays a key role in defining the design. Few factors that are needed to be considered for the meterial selection process are, geometrical constraits, environmental factors and strength requirements. Specifications such as heat treatment, material properties, impact propertied and other factors have to be a part of the design. As the focus for this section is only on presenting a model for the design and not on the actual component, a samle meterial is chosen for demonstrating the model. Though for the actual design in case of a hydro-kinetic turbine, ket factors for the material would be high corrosion resistance, strength requirement based on geometical consraints, reliability target, etc.

3.5. SHEAR FORCE, BENDING MOMENT, AND SHEAR AND DIRECT STRESS

Figure 3-6 illustrates the loads and reactions acting on the shaft at different sections. R_1 and R_2 are the reactions at bearings 1 and 2 respectively. The blade weight is neglected in the analysis because it has little effect when the equipment is submersed in water. The thrust from the blades is taken by bearing 2.

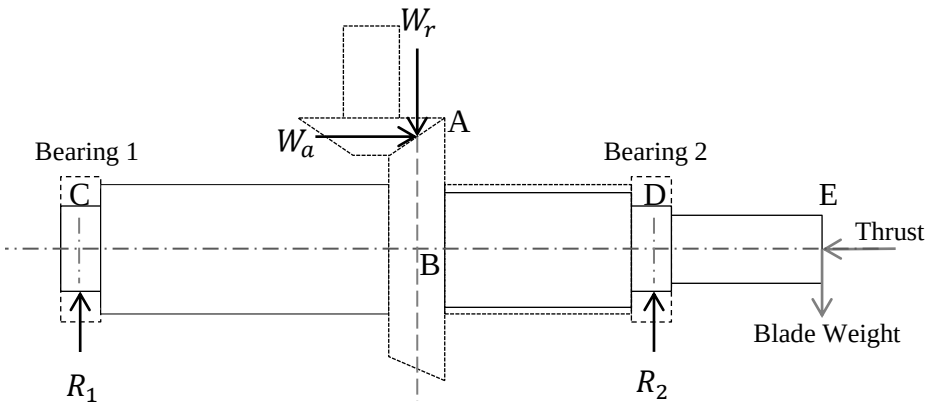

Figure 3.6. Transverse and axial loading on the shaft

Diameters of different sections of the shaft as in Figure 3-5 are only used to provide for axial alignment of the shaft elements and to take minor thust loads. The diameters of the sections are to be ateast the minimum safe design diameter for the operation of the transmission shaft. Hence the transmission shaft in Figure 3-6 is modeled into a shaft of uniform circular cross-section of minimum diameter *d*. Now the load W_a at the contact point A is translated into a bending moment M_b and a axial force W_b at point B; $M_b = W_a.r_a$, $W_b = -W_a$. Length of the shaft between C and B is l_1 and B and D is l_2. From Figure 3-7, reactions at the bearings are calculated by taking moments form one of the points on the shaft. For instance, reaction R_1 is computed by taking moments at D;

$$R_1 = \frac{l_2 W_r - M_B}{(l_1 + l_2)} \tag{3.28}$$

Now adding all the transverse forces on the shaft and equating them to zero, R_2 can be calculated as

$$R_2 = W_r - \frac{l_2 W_r - M_B}{(l_1 + l_2)} = \frac{l_1 W_r + M_B}{(l_1 + l_2)} \tag{3.29}$$

where Axial reaction forces at C and D are $A_1 = -W_b$ and $A_2 = -F_T$

From the bending moment diagram in Figure 3-7, the maximum bending occurs at point B and is

$$M_{max} = \frac{l_2 l_1 W_r - l_1 M_B}{(l_1 + l_2)} + M_B = \frac{l_2 l_1 W_r + l_2 M_B}{(l_1 + l_2)} \tag{3.30}$$

The maximum shear force is also at section C which is eigther R_1 or R_2 which is based on the lengths l_1 and l_2. From bending moment diagram in Figure 3-7 and Equation (3.30), it can also be seen that the maximum bending moment is derectly proportional to the distance l_1 and mean the gear tooth radius r_a. Hence it is obvious that both these dimentions need to be as minimum as possible.

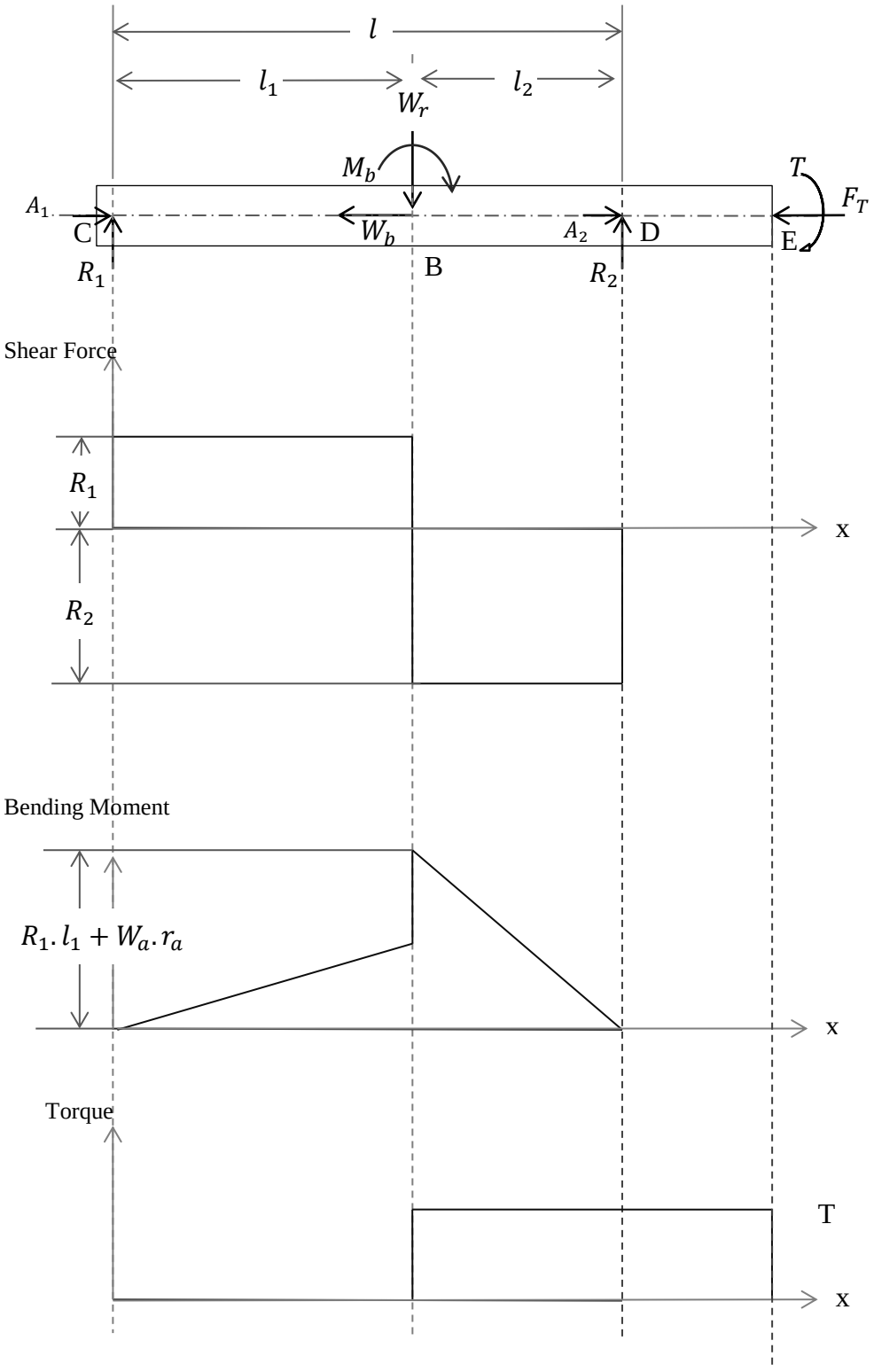

Figure 3.7. Free body, shear force, bending moment and torque diagrams

3.6. STRESS AND DEFLECTION ANALYSIS

3.6.1. Stress Analysis. Form Figure 3-7, from the stress point of view, section C has the highest bending moment and hence stress analysis is done for section C. The maximum stress due to bending at a section can be determined using Flexure formula using the following equation:

$$\sigma_{BM} = \frac{M_{max} K_t}{S} \tag{3.31}$$

where *S* is the section modulus.

For a circular shaft, S is $\frac{\pi D^3}{32}$ and K_t is stress concentration factor. A stress concentration factor is used to analyze beams with change in cross-section. For section C, a stress concentration factor for the keyseat is to be applied.

The force W_b acting at section C in the axial direction causes a direct tensile stress and the magnitude of the direct compression stress is computed as

$$\sigma_C = \frac{W_b}{A} \tag{3.32}$$

where *A* is the cross-sectional area at the section.

It can be reasoned that this compression stress adds up to the stress due to bending at top face of the shaft because the nature of stress due to either of them is compressive at the top face. Hence the total shear stress σ_T at C is sum of σ_{BM} and σ_C and is

$$\sigma_T = \frac{M_{max} K_t}{S} + \frac{W_b}{A} \tag{3.33}$$

Torsional shear stress τ at a section is given by

$$\tau = \frac{T}{Z_p} \tag{3.34}$$

where $Z_p = \frac{\pi D^3}{16}$ is the polar moment of inertia for circular section.

We observe that the three loadings M_{max}, W_b and T occur at the same surface is scrutiny. By using Mohr's circle it can be shown that the two nonzero principle stresses σ_a and σ_b are

$$\sigma_a, \sigma_b = \frac{\sigma_T}{2} \pm [(\frac{\sigma_T}{2})^2 + \tau^2]^{\frac{1}{2}} \tag{3.35}$$

These principle stresses are combined, and using distortion-energy theory, von Mises stress σ' can be written as

$$\sigma' = (\sigma_a^2 - \sigma_a\sigma_b + \sigma_b^2)^{\frac{1}{2}} = (\sigma_T^2 + 3\tau^2)^{\frac{1}{2}} \tag{3.36}$$

and using the Maximum-shear theory

$$\tau_{max} = \frac{\sigma_a - \sigma_b}{2} = \frac{1}{2}(\sigma_T^2 + 4\tau^2)^{\frac{1}{2}} \tag{3.37}$$

By substituting σ_T and τ in Equations (3.36) and (3.37), we obtain

$$\sigma' = [(\frac{M_{max}K_t}{\frac{\pi D^3}{32}} + \frac{W_b}{\frac{\pi D^2}{4}})^2 + 3\left(\frac{T}{\frac{\pi D^3}{16}}\right)^2]^{\frac{1}{2}} \tag{3.38}$$

$$\tau_{max} = \frac{1}{2}[(\frac{M_{max}K_t}{\frac{\pi D^3}{32}} + \frac{W_b}{\frac{\pi D^2}{4}})^2 + 4\left(\frac{T}{\frac{\pi D^3}{16}}\right)^2]^{\frac{1}{2}} \tag{3.39}$$

Any of the Equations (3.36) or (3.37) can be compared with the material strength to determine diameter D.

3.6.2. Deflection Analysis. Material distortion cannot be avoided under load. In design practice usually there is a choice to design for strength and check for distortion or to design for distortion and check for strength. In case of power transmission, there is an active distortion constraint set due to deflection limits at the bearings. Hence design based on distortion and later checking for strength is also appealing. An equation for slope at the bearings is taken from [21] and is given as

$$\theta_C = \frac{1}{6EIl}[W_r l_2(l_2^2 - l^2) + M_b(6l_1 l - 2l^2 - 3l_1^2)] \quad (3.40)$$

$$\theta_D = \frac{1}{6EIl}[W_r l_1(l^2 - l_1^2) + M_b(l^2 - 3l_1^2)] \quad (3.41)$$

where E is the modulus of elasticity and $I = \frac{\pi D^4}{64}$ is the moment of inertia at the section. Now Equations (3.40) and (3.41) can be used to compare with the allowable defection to determine the diameter of the shaft.

3.7. SPECIFY MINIMUM SHAFT DIAMETER

The method discussed so far in chapter 3 is now applied to a sample turbine specification for demonstration. The following are the input variables necessary for the model.

3.7.1. Characteristics of the system:

- Maximum water velocity (V_0) 4 m/sec
- Blade Pitch (θ_P) 15-45 degrees
- Rotor radius (r) 0.5 m
- Maximum rotor Speed (ω) 400 rpm
- Density (ρ) 1000 kg/m^3

- Number of blades (*B*) 3
- Hydrofoil

A hydrofoil profile consists of the specifications of the profile of the blade. This includes chord length and twist along different sections of the blade.

Table 3.1. Chord length and twist of blade vs. position

Position	Chord Length (c)	Chord Twist
0.2	0.225	25
0.35	0.165	18
0.45	0.116	15
0.55	0.091	10
0.65	0.067	6
0.85	0.056	2
0.95	0.063	1

The transmission shaft is to be designed to transmit torque in a perpendicular axis without any speed step. The Number of teeth on gear = number of teeth on pinion. Hence a Miter gear is used for this application. Based on the dimensions of the blade a rough pitch diameter is assumed in order to determine the approximate shaft diameter and then the exact gear specifications are determined based on the approximate shaft diameter.

For instance, pitch radius of the gear (r_a)= 0.065 m, Pressure angle = 20 degrees

Based on the gear diameter, the length of the shaft and positioning of the gear are also assumed. These dimensions are reiterated from the approximate shaft diameter.

- l_1= 0.15 m
- l_2= 0.15 m

3.7.2. Shaft Material. For the material selection and specification, it is necessary to consider many aspects such as the working environment and loading type. Hence in-depth study is necessary. A few key characteristics are outlined for material selection such as

- Resistance to corrosion
- Resistance to oxidation
- Ease of fabrication
- High strength with low weight
- Ready availability of a wide range of product forms

Based on these characteristics stainless steel is considered because of its use in similar application. For marine applications, nickel based alloys called austenitic are usually preferred for their high corrosion resistance. Austenitic stainless steels are identified by their 300-series designation.

Grade 316 is the standard molybdenum-bearing grade, second in importance to 304 amongst the austenitic stainless steels. The molybdenum gives 316 better overall corrosion resistant properties than Grade 304, particularly higher resistance to pitting and crevice corrosion in chloride environments. It has excellent forming and welding characteristics. It is readily brake or roll formed into a variety of parts for applications in

the industrial, architectural, and transportation fields. Hence 316 Stainless Steel is chosen for this application. Its key properties

- Tensile Strength min (S_u) = 515 (MPa)
- Yield Strength min (S_y) = 205 (MPa)
- Elastic Modulus (E) = 193 (GPa)

Stress concentration factor for the keyway is taken from [22], K_t = 3.4

All the input variables necessary for the design are specified. Now limit-state functions are to determined based on Equations (3.38) through (3.41)

From the stress analysis using distortion-energy the stress is compared to allowable material stress to determine the design diameter. For a design factor of n_d an allowable stress is given by

$$\sigma'_{al} = \frac{S_y}{n_d} \tag{3.42}$$

Comparing the allowable stress from Equation (3.42) to stress from Equation (3.38) the limit-state function 1 is given by

$$\sigma'_{al} \geq \sigma' \tag{3.43}$$

$$\frac{S_y}{n_d} - \left(\left(\frac{M_{max}K_t}{\frac{\pi D^3}{32}} + \frac{W_b}{\frac{\pi D^2}{4}}\right)^2 + 3\left(\frac{T}{\frac{\pi D^3}{16}}\right)^2\right)^{\frac{1}{2}} \geq 0 \tag{3.44}$$

Now using Equation (3.37) for the maximum shear theory, the maximum shear is compared with allowable shear given by $\tau_{al} = \frac{S_y}{2n_d}$ to determine the limit-state function for maximum shear

$$\tau_{al} \geq \tau_{max} \tag{3.45}$$

$$\frac{S_y}{2n_d} - \frac{1}{2}\left(\left(\frac{M_{max}K_t}{\frac{\pi D^3}{32}} + \frac{W_b}{\frac{\pi D^2}{4}}\right)^2 + 4\left(\frac{T}{\frac{\pi D^3}{16}}\right)^2\right)^{\frac{1}{2}} \geq 0 \tag{3.46}$$

Similarly based on the deflections at bearings C and D two more limit-state functions can be determined. The maximum allowable deflection at a bearing depends on the type of bearings. For instance, the slope of the shaft centerline with respect to a rolling-bearing outer ring centerline ought to be less than 0.001 rad for cylindrical and 0.0005 for tapered roller bearings. For the application because of the nature of forces at the bearings (like thrust and radial) a tapered roller bearing is a good choice as they can handle thrust loads. So, using Equations (3.40) and (3.41) the deflection should be less than 0.0005 rad.

$$0.0005 \geq \theta_C;\ 0.0005 \geq \theta_D \tag{3.47}$$

$$0.0005 - \frac{1}{6Eil}\left[W_r l_2 (l_2^2 - l^2) + M_b (6l_1 l - 2l^2 - 3l_1^2)\right] \geq 0 \tag{3.48}$$

$$0.0005 - \frac{1}{6Eil}\left[W_r l_1 (l^2 - l_1^2) + M_b (l^2 - 3l_1^2)\right] \geq 0 \tag{3.49}$$

Equations (3.46) and (3.47) are re-written as

$$D - \left(\frac{64\left[W_r l_2 \left(l_2^2 - l^2\right) + M_b \left(6l_1 l - 2l^2 - 3l_1^2\right)\right]}{0.003El\pi}\right)^{\frac{1}{4}} \geq 0 \tag{3.50}$$

$$D - \left(\frac{64\left[W_r l_1 \left(l^2 - l_1^2\right) + M_b \left(l^2 - 3l_1^2\right)\right]}{0.003El\pi}\right)^{\frac{1}{4}} \geq 0 \tag{3.51}$$

A conservative dimension for the shaft diameter is determined from the limit-state functions (3.44), (3.46), (3.50) and (3.51). For the above configuration, loads on the shaft are:

- Torque = 221.3431 Nm
- Thrust = 77.4228 N
- W_r = 876.4024 N
- W_a = 876.4024 N

W_r and W_a are equal in magnitude because of the Miter gear (number of teeth on gear is equal to number of teeth on pinion)

Shaft diameters based on the four failure modes have been determined. The following are the diameters with respect to each of the failure criteria:

Table 3.2. Deterministic design Results

Design Criteria	Shaft Minimum Diameter
Distortion-energy theory	0.033 m
Maximum shear theory	0.0308 m
Allowable deflections at bearing C	0.0307 m
Allowable deflections at bearing D	0.0330 m

3.8. SHAFT FATIGUE LIFE

Failure due to fatigue is an important aspect to be taken into consideration in component or system design. It is observed in many cases that the actual maximum

stresses is well below ultimate strength of material, and in some cases is even below the material yield strength. This is mostly because of the repetitive nature of loading causing failure due to fatigue.

It is essential to determine the endurance limit S_e to quantify the fatigue characteristics of a component. To determine the endurance limit it is necessary to consider a number of properties like material properties, manufacturing properties, environmental properties and design properties. Marin equation from [21] is for endurance limit calculation:

$$S_e = k_a k_b k_c k_d k_e k_f S'_e \tag{3.52}$$

where

k_a= surface condition modification factor

k_b= size modification factor

k_c= load modification factor

k_d= temperature modification factor

k_e= reliability factor

k_f= miscellaneous-effects modification factor

S'_e= rotary-beam test specimen endurance limit = $0.504 S_{ut}$

If the maximum stress is below the endurance limit, then the component can withstand infinite cycles. But if the maximum stress is between the yield strength of the material and the endurance limit, we may have finite life. Different approaches to determine the lifecycle of the component can be used to determine the fatigue life.

4. RELIABILITY ANALYSIS FOR THE SHAFT DESIGN

4.1. INTRODUCTION

The objective of the section is to determine the reliability of the deterministic design and then to improve the design to satisfy the reliability requirement. To design a component based on certain reliability standard demands for more accurate means of modeling the practical application. For example, in deterministic design the variations in the river velocity are not accounted for. The deterministic design is done with the mean values of the variables taken into consideration. For this reason a reliability analysis is to be performed to see if the design will fail or if the design meets the reliability requirement of the component in given range of conditions for a specific period.

Random variables can be broadly classified as time-invariant and time-dependent random variables. Time-invariant random variables as suggested by its name do not change over time. On the other hand time-dependent random variables are a stochastic process explicit to time. Reliability analysis involving time-dependent random variables is consequently called time-dependent reliability. In case of the transmission shaft design, some of the time-invariant random variables would be the material strength, geometrical dimensions of the shaft and so forth. The river velocity in contrary varies both in space and time. The variation in river velocity with reference to the position on cross-section of the river is challenging to model especially for large rivers with large cross-sectional area and river flow velocities greater than 1m/s [23]**.** As a result, the data regarding the spatial variations of the river velocity is generally unavailable. For this reason, the spatial variation of the river flow velocity is neglected in the analysis. But, in case of large turbine blade diameter, this might cause a potential bending moment due to the velocity

profile. An illustration of this scenario is presented in Figure 4.1. Fortunately, time sensitivity of the river flow however is recorded and can be used to derive statistical data of river flow with respect to time. The data were used to model the river flow velocity as a stochastic process.

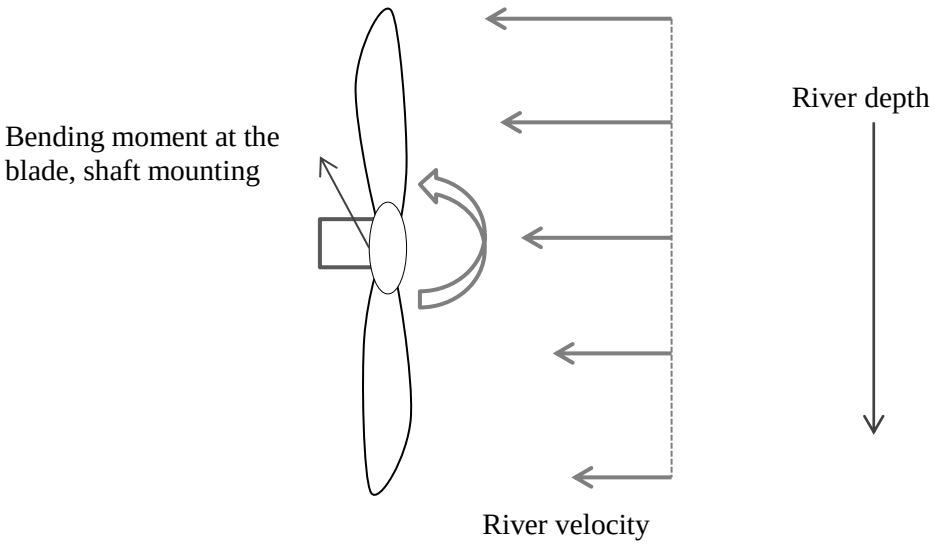

Figure 4.1. Bending moment due to variation in river velocity with depth

The reliability of the transmission shaft was determined using the four failure modes described in the deterministic design section. After the reliability of the shaft was accessed, reliability-based design (RBD) was performed using time-dependent reliability by Sampling Approach to Extreme Values of Stochastic Process (SAEVSP) [24] to compare and contrast with the deterministic design. The procedure followed is elaborated and the results are analyzed in the sections that follow:

4.2. RIVER VELOCITY MODELING

As discussed earlier, the river flow velocity with relative to time could be modeled but not the positional variation. This is because of the unavailability of a mathematical model governing the positional variation. The hydrokinetic turbine is designed to be portable and to be able to be placed at any location along the river and hence it is difficult to predetermine at which location the velocity should be considered.

A similar procedure followed by Zhen and Du [24], was used for the river velocity modeling. The river flow velocity was modeled using the data of river discharge. From the Manning-Strikler formula [25]**,** for a site, the cross-sectional average river flow velocity is governed by the equation [26] [27]

$$v(t) = n^{-1}H(t)^{2/3}S^{1/2} \tag{4.1}$$

where $v(t)$ is the river flow velocity, n is the river bed roughness, $H(t)$ is the hydraulic radius, and S is the river slope. The hydraulic radius is presented using depth D and width W, considering a rectangular river bed as following:

$$H(t) = \frac{DW}{(2D+W)} \tag{4.2}$$

Allen [28] has found a relation between discharge d_m, depth D and width W using the following equations introduced by Leopold and Maddock [29], after a research on 674 river cross-sections across USA and Canada.

$$W = 2.71d_m^{0.557} \tag{4.3}$$

and

$$D = 0.349d_m^{0.341} \tag{4.4}$$

If the river bed slope and roughness are given, then the river velocity is a function of river discharge. Hence statistical characteristics of the river velocity are directly governed by the river discharge.

The statistical characteristics of the discharge are determined per month because of low variations in the river discharge. From [30] and [31] the monthly river discharge follows a lognormal distribution. So, the cumulative distribution function (CDF) $F_M(d_m)$ is given by

$$F_M(d_m) = \Phi\{\frac{[\ln(d_m) - \mu_M(t)]}{\sigma_M(t)}\} \tag{4.5}$$

For the design, historical river discharge data of the Missouri river from 1897 to 1988 at Hermann, Missouri station [32] is used. From the data, the mean $\mu_M(t)$ and standard deviation $\sigma_M(t)$ of the river discharge were fit as a function of time *t* as:

$$\mu_M(t) = a_0^m + \sum_{i=1}^{5}[a_i^m \cos(iw_m t) + b_i^m \sin(iw_m t)] \tag{4.6}$$

and

$$\sigma_M(t) = a_0^s + \sum_{j=1}^{5}[a_i^s \cos(iw_s t) + b_i^s \sin(iw_s t)] \tag{4.7}$$

where

$a_0^m = 2335, a_1^m = -1076, a_2^m = 241.3, a_3^m = 61.69, a_4^m = -30.92, a_5^m = 32.38,$

$b_1^m = 57.49, b_2^m = -174.9, b_3^m = -296.2, b_4^m = 213.6, b_5^m = -133.6, w_m = 0.5583$

$a_0^s = 1280, a_1^s = -497.2, a_2^s = 145.8, a_3^s = 225.4, a_4^s = -203.1, a_5^s = 99.47,$

$b_1^s = -82.58, b_2^s = -19.06, b_3^s = -178.7, b_4^s = 36.15, b_5^s = -52.47, w_s = 0.5887$

and according to the "over time' autocorrelation function of the Elde River [31], the auto correlation function of monthly discharge of Missouri river was assumed as

$$\rho_M(t_1, t_2) = \exp\{-\left[6\left(\frac{t_1 - t_2}{5}\right)\right]^2\} \tag{4.8}$$

4.3. TIME-DEPENDENT RELIABILITY ANALYSIS

As discussed earlier, time-dependent reliability is the probability that a component or a system does not fail in the given period of time. Reliability is time dependent when any variables or the system as a whole is explicit with respect to time. Due to these time dependent uncertainties, the reliability of the system or component often decreases with time. In the case of the transmission shaft the only random variable sensitive to time is the river velocity as conferred in the previous section.

A limit-state function is a function of random variables and stochastic process used to determine the state of safety or failure of the system. In case of the shaft design, the limit-state function is of the form

$$Z = g\big(\boldsymbol{X}, \boldsymbol{Y}(t)\big) \tag{4.9}$$

where $\boldsymbol{X}$ and $\boldsymbol{Y}(t)$ are time-invariant and time-dependent random variables, respectively. $g(.)$ is the limit-state function, and Z is the response variable. Equation (4.9) is the general form; From Equation (3.42) the limit-state function can be rewritten as

$$Z = g\left(S_y, D, l_1, l_2, R, r_{a,} V(t)\right) \tag{4.10}$$

Many time-dependent reliability analysis methodologies are available presently to analyze the limit-state function of the form in equation (4.9). Few of the methods include:

- Monte Carlo simulation (MCS) [12],

- Gamma process method [33],
- Markov chain method [34],
- Upcrossing rate method [35] [36],
- Sampling approach to extreme values of stochastic process (SAEVSP) method [24].

Amongst these methods the upcrossing rate method is the most popular method. The advantage of this method amongst other methods is its efficiency, but its accuracy may be poor [37]. This is due to the assumption that all the upcrossing are statistically independent. This is conservative and can lead to large errors. Though few modifications have been proposed to remedy this, they are limited to special problems. MCS is the most accurate method to use but is computationally expensive due to large of function calls. In our case the computational cost might not be high. This is because our models do not involve intensive simulations. MCS was therefore done for comparison to the method followed. Since the SAEVSP method proposed by Zhen and Du [24] is based on First Order Reliability Method (FORM) and is as accurate and efficient as FORM. We used SAEVSP for reliability analysis.

4.3.1. Sampling Approach to Extreme Values of Stochastic Process. This method is based on the idea to replace the stochastic process in the limit-state function with the distribution of extreme values of the stochastic process to convert the time-dependent limit-state function into its time-invariant counterpart. For the limit-state function in Equation (4.2) as the velocity of water $\boldsymbol{V(t)}$ increases the function $\boldsymbol{g(.)}$ decreases and hence the extreme value to be used from sampling should be the maximum velocity at different time intervals. In case the yield strength is a stochastic process then as the yield strength increases, the function $\boldsymbol{g(.)}$ increases; so the minimum values of the samples of a given time interval are considered for generating a cumulative distribution function (CFD).

This new method is performed in two stages. The first stage is approximating the distribution of $V(t)$ by Monte Carlo Simulation. The second stage is time invariant reliability analysis. A flow cart of the method is described in Figure 4.2.

Stage 1: Estimating the distribution of the maximum values of the river flow velocity $V(t)$.

To estimate the distribution, the first step is to generate samples and then identify the extreme values. To do this, the time interval under consideration $[0, t_s]$ is divided into N equal small intervals. $V(t_i)$, $(i = 0,1, \dots, N)$ is a random variable at t_i. Now n random samples are generated for each $V(t_i)$. Now we need to identify the maximum values

$$w_j = \max(\mathrm{V}(t_i))_{i=0,1,\dots,N} \tag{4.11}$$

Now the j samples of the maximum velocity generated are used to estimate the CDF $F_V(w)$. This is done using saddlepoint approximation. Once the distribution of the maximum velocity is known, $V(t)$ is replaced with the new time-invariant random

variable W generated from the above method. More in-depth details about the procedure for approximating CDF of W and using saddle point approximation can be found in [24]**.** Now the time dependent limit-state function is transformed into its time-invariant counterpart. The traditional FORM can be then used to analyze the reliability of the shaft. FORM is performed in two steps, transformation and linearization. We first need to transform the random variables into standard normal variables. Now the time invariant limit-state function is transformed as

$$Y = g\left(S_y, D, l_1, l_2, R, r_a, W\right) = g'\left(U_{S_y}, U_D, U_{l_1}, U_{l_2}, U_R, U_{r_a}, U_W\right) \tag{4.12}$$

Where $U_{S_y} = \frac{(S_y - \mu_{S_y})}{\sigma_{S_y}}$, in which $\mu_{S_y}$is the mean and σ_{S_y} is the standard deviation of yield strength respectively. $U_D = \frac{(D-\mu_D)}{\sigma_D}$, in which $\mu_D$is the mean and σ_D is the standard deviation of design diameter respectively. $U_{l_1} = \frac{(l_1 - \mu_{l_1})}{\sigma_{l_1}}$, in which $\mu_{l_1}$is the mean and σ_{l_1} is the standard deviation of length l_1 respectively. $U_{l_2} = \frac{(l_2 - \mu_{l_2})}{\sigma_{l_2}}$, in which $\mu_{l_2}$is the mean and σ_{l_2} is the standard deviation of length l_2 respectively. $U_R = \frac{(R-\mu_R)}{\sigma_R}$, in which $\mu_R$is the mean and σ_R is the standard deviation of rotor radius respectively. $U_{r_a} = \frac{(r_a - \mu_{r_a})}{\sigma_{r_a}}$, in which $\mu_{r_a}$is the mean and σ_{r_a} is the standard deviation of bevel gear radius respectively. $U_W = \frac{(W-\mu_W)}{\sigma_W}$, in which $\mu_W$is the mean and σ_W is the standard deviation of extreme values of river velocity respectively.

$g'(\mathrm{U})$ is usually non-linear. Even if the function g(X)is linear, the function $\mathrm{g}'(\mathrm{U})$ may still be non-linear because the X to U transformation is nonlinear. Hence $\mathrm{g}'(\mathrm{U})$ is approximated using first order Taylor series and the most probable point (MPP) on the

function is determined using the MPP search algorithm [24]. The MPP u^* is now used to determine the probability of failure P_f. The reliability of the shaft is therefore $1 - P_f$.

$$\beta = \| u^* \| = \sqrt{\sum_{i=1}^{7} (u_i^*)^2} \tag{4.13}$$

$$P_f = \Phi(-\beta) \tag{4.14}$$

where $(u_1^*, u_2^*, u_3^*, u_4^*, u_5^*, u_6^*, u_7^*)$=($u_{S_y}^*, u_D^*, u_{l_1}^*, u_{l_2}^*, u_R^*, u_{r_a}^*, u_W^*$).

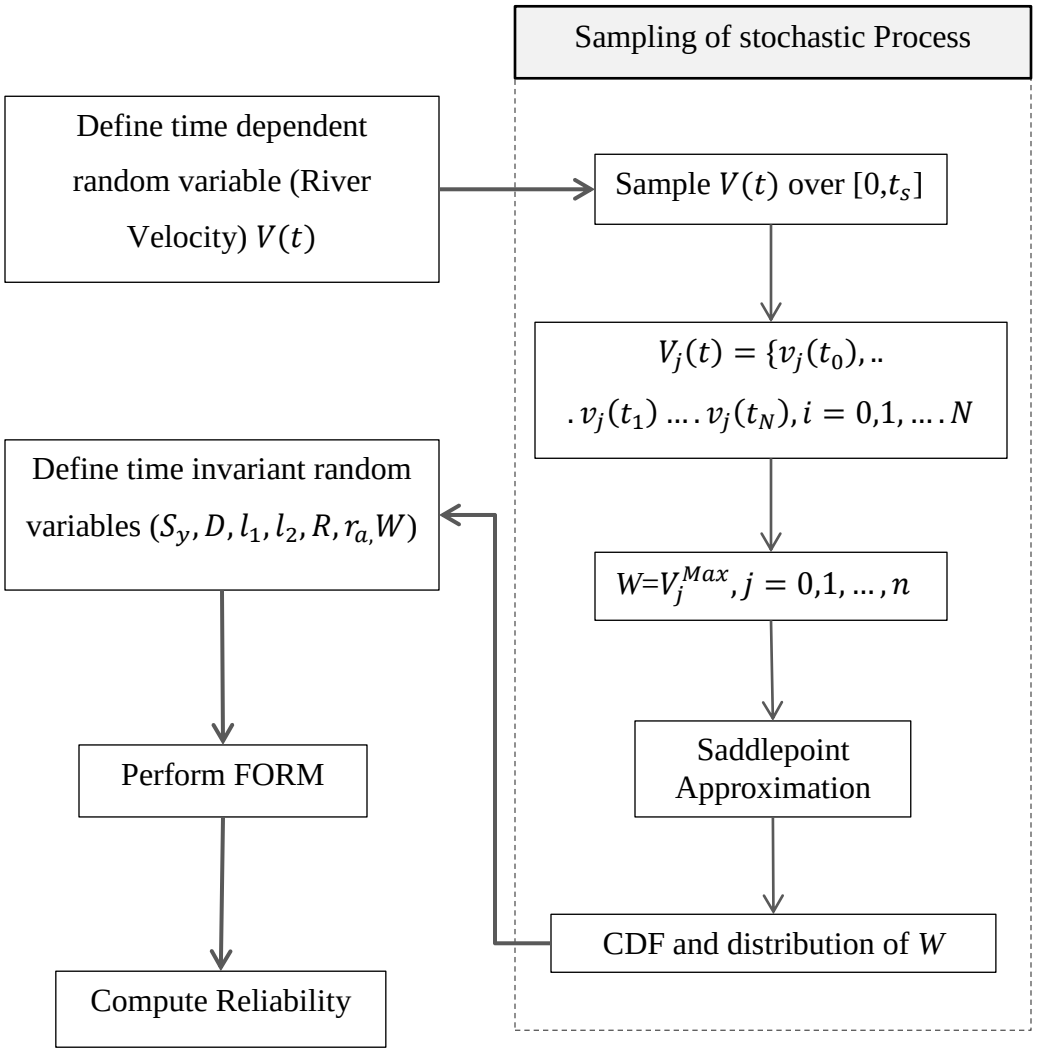

Figure 4.2. Flow chart of the time dependent reliability analysis

4.3.2. Monte Carlo Simulation (MCS). Monte Carlo simulation was performed to evaluate the accuracy of the previously discussed method. But, MCS is only accurate if a large number of simulations are performed. Hence the accuracy is directly related to the number of simulations and is also directly proportional to the computational cost. In order to reach a desirable level of confidence, the computational requirement is so high that using MCS is no longer feasible.

A brief procedure followed to conduct the time-dependent MCS is discussed. First, the time interval under consideration was split into *n* different time intervals. For our case it was split into months. Now *S* samples of the river velocity are generated at each sub time interval. This was done using the velocity modeling discussed earlier. Now $n \times S$ samples were generated for the time-invariant random variables and then, the function $g\left(S_y, D, l_1, l_2, R, r_a, V(t)\right)$ was evaluated. Based on the performance function, the statistical analysis on the output was performed. Number of failure conditions N_F was accounted and the corresponding reliability was determined. An outline flowchart of the MCS is shown in Figure 4.3. The reliability is given by

$$R = 1 - \frac{N_F}{n \times S} \tag{4.15}$$

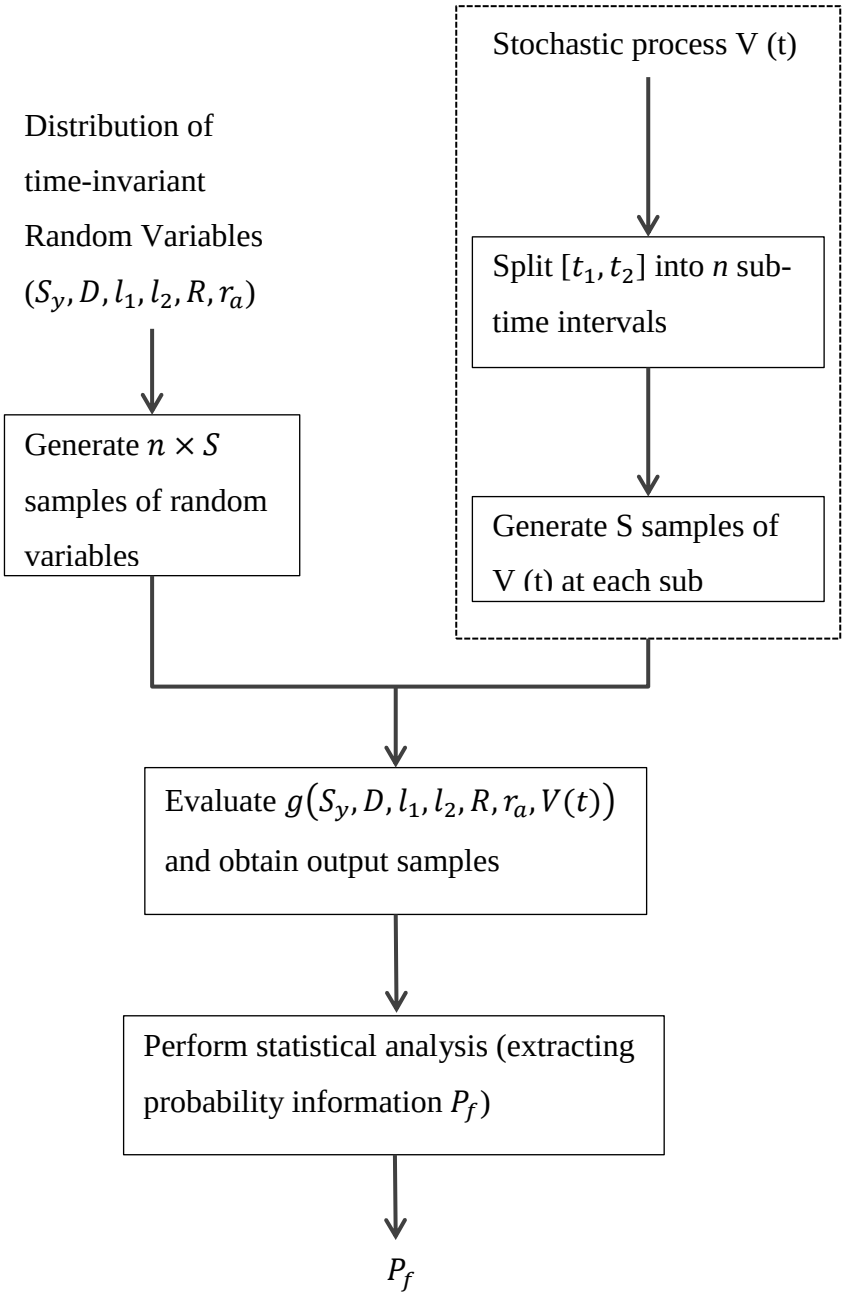

Figure 4.3. MCS procedure for time dependent reliability analysis

4.3.3. Limit-State Functions. The four limit-state functions are defined as follows:

4.3.3.1 Based on the strength theories

From the distortion-energy:

$$g_{DE} = \frac{S_y}{n_d} - ((\frac{M_{max}K_t}{\frac{\pi D^3}{32}} + \frac{W_b}{\frac{\pi D^2}{4}})^2 + 3(\frac{T}{\frac{\pi D^3}{16}})^2)^{\frac{1}{2}} \quad (4.16)$$

Maximum shear theory:

$$g_{MS} = \frac{S_y}{2n_d} - \frac{1}{2}((\frac{M_{max}K_t}{\frac{\pi D^3}{32}} + \frac{W_b}{\frac{\pi D^2}{4}})^2 + 4(\frac{T}{\frac{\pi D^3}{16}})^2)^{\frac{1}{2}} \quad (4.17)$$

4.3.3.2 Based on allowable deflection

Maximum allowable deflection at a bearing C:

$$g_{DC} = D - (\frac{64[W_r l_2(l_2^2 - l^2) + M_b(6l_1 l - 2l^2 - 3l_1^2)]}{0.003El\pi})^{\frac{1}{4}} \quad (4.18)$$

Maximum allowable deflection at a bearing D:

$$g_{DD} = D - (\frac{64[W_r l_1(l^2 - l_1^2) + M_b(l^2 - 3l_1^2)]}{0.003El\pi})^{\frac{1}{4}} \quad (4.19)$$

All the limit-state functions discussed are defined as failure if $g < 0$. From the deterministic design, the shaft diameter based on the distortion energy theory and the maximum allowable deflection at C yield higher shaft diameter. For this reason, limit-state functions g_{DE} and g_{Dc} are used as criteria for reliability analysis. The input variables necessary for the limit-state functions g_{DE} and g_{Dc} are listed below.

4.3.4. Design Inputs. All the input variables used in the reliability analysis are classified into deterministic, random variables and stochastic process (river velocity). All the variables were considered to have a mean value equal to deterministic design input except for the river velocity. The deterministic design was performed for maximum limit of river velocity.

4.3.4.1 Deterministic variables

- Water Density, ρ = 1000 kg/m^3
- Tip speed ratio, λ = 5
- Blade pitch, θ_p = 15
- Twist of blade, β = Table 3.1
- Chord Length, c = Table 3.1
- Pressure angle, ϕ = 20
- Number of blades, B = 3
- Number of gear tooth N_G, N_P = 30
- Rotor radius, R = 0.5 m

4.3.4.2 Random variables. As discussed earlier, the deterministic design inputs are used as means for the random variables correspondingly. The standard deviation for the dimension variables is taken as one third of the manufacturing tolerance limit [38].

Table 4.1. Radom variables for reliability Analysis

Variable	Mean	Standard Deviation	Distribution
Diameter, D	0.033m	0.0001m	Normal
Yield Strength, S_y	205 MPa	20 MPa	Normal
Elastic Modulus, E	193 GPa	10 GPa	Normal
Length, L1	0.15m	0.0001m	Normal
Length, L2	0.15m	0.0001m	Normal
Gear Radius, Ra	0.065m	0.0001m	Normal

For the river velocity sampling, a constant mean of 3 m/sec and standard deviation of 0.5m/sec are considered. This because the velocity model discussed is not accurate for longer time span. The radius of the rotor, R is considered as a deterministic variable for computational ease while using MCS and the variation in the reliability analysis because of this assumption is also discussed in the results section.

4.4. RELIABILITY-BASED DESIGN OPTIMIZATION (RBDO)

Reliability-based design Optimization (RBDO) is a design methodology used to obtain optimal designs characterized by the reliability target. The reliability-based design takes into account these uncertainties of the involving variables and hence provide a more reliable and safe design.

The main steps involved in the RBDO include characterizing the important random variables and the failure modes. Uncertainty is generally characterized using probability theory. The probabilistic distributions of random variables are obtained using statistical models. When designing a component with multiples failure modes, it is

important to make it reliable with respect to each of the failure modes. In a reliability-based design formulation, the failure modes are considered as constraint functions with respect to their probabilities of failure. The probability of failure corresponding to each failure mode is computed by performing probabilistic reliability analysis. Reliability analysis methods discussed earlier are used to calculate the probability of failure.

A typical RBDO model for a single design variable is expressed as:

$$\begin{cases} Minimize\ objective\ (d) \\ Subject\ to \\ P\{g(\boldsymbol{X}, \boldsymbol{Y}(t), d) > 0\} \geq R_T \\ F_i(d) \leq 0, i = 1,2, \dots, N \\ d_l \leq d \leq d_u \end{cases} \tag{4.20}$$

where d is the design variable, $\boldsymbol{X}$ is the vector of random variables and $\boldsymbol{Y}(t)$ is the vector of the stochastic processes if any. The objective of this RBDO model is to minimize a function of the design variable. $g(.)$ is the performance function and $F_i(d)$ are the inequality constraints to be considered during the design optimization which are the constraints that should be satisfied during the optimization. R_T is the target reliability and d_l and d_u are the lower limit and the upper limit for the design variable.

In case of the time dependent reliability- based design, the reliability is assessed using the SAEVSP described in section 4.3.1. Optimization was performed using Matlab. A flow chart describing a brief outline of the time dependent reliability design methodology followed is illustrated in Figure 4.4.

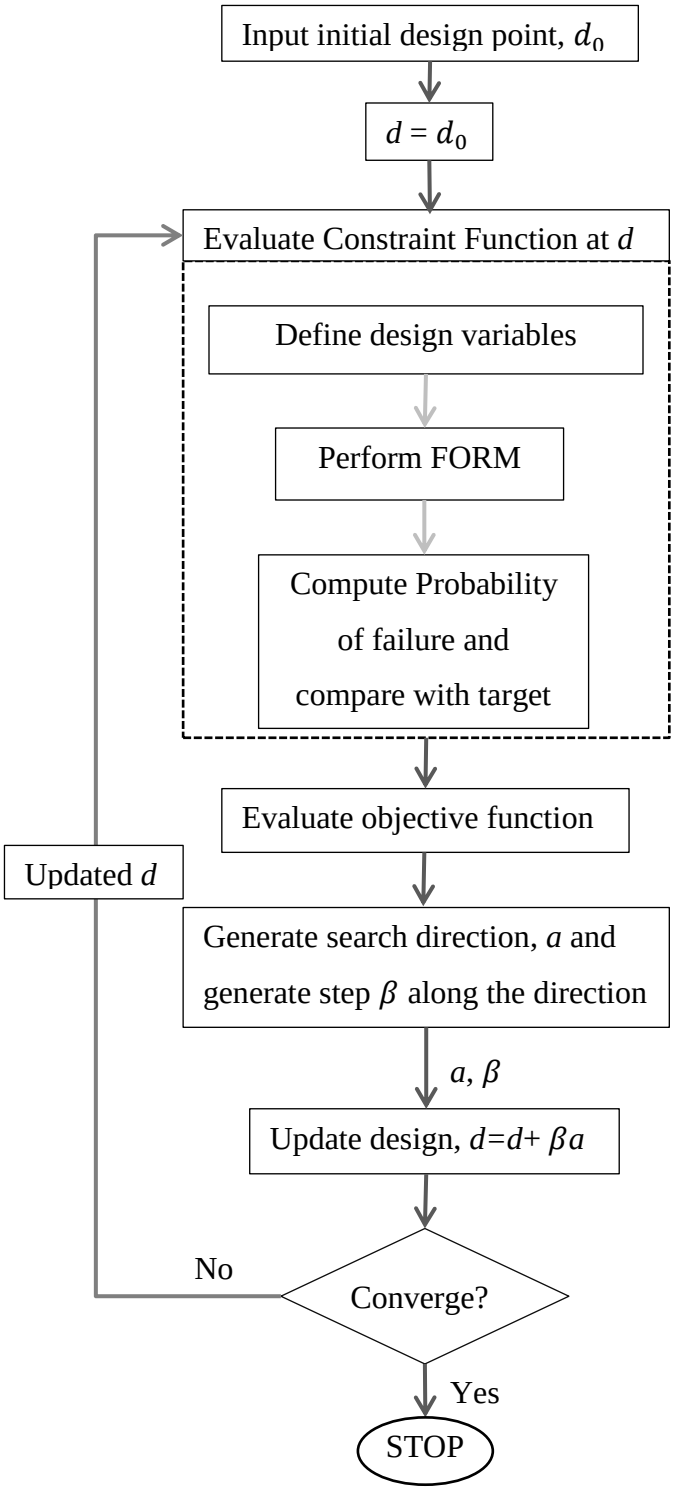

Figure 4.4. Reliability-based design optimization

4.5. RELIABILITY ANALYSIS RESULTS

Reliability analysis was performed using the limit-state functions in Equations (4.16) and (4.19) because the deterministic design yielded a higher diameter when designed using these failure criteria. The diameter from the deterministic design is 0.033m.

As discussed in the previous sections SAEVSP method and MCS were performed for both limit-state functions in order to evaluate the SAEVSP method for its accuracy. The probability of failure was evaluated over a time span of 20 years. A layout of the results and discussion done in this section is presented in Figure 4.5.

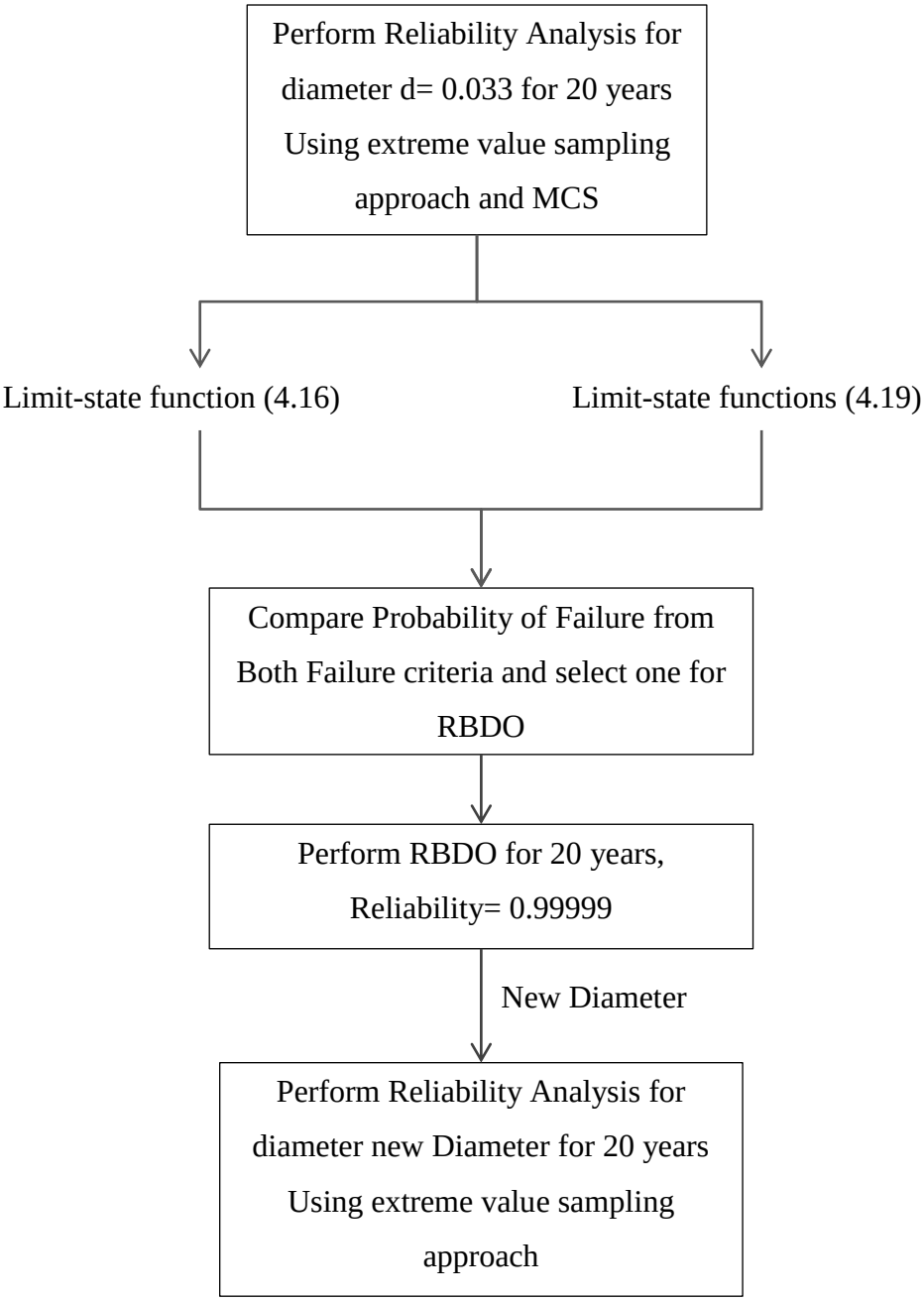

Figure 4.5: Outline of the reliability analysis and RBBO

The results in Table 4.2 show the probability of failure obtained from SAEVSP, compared with MCS for a time span of 20 years. The distributions of the random variables involved in the analysis are in Table 4.1.

Equation (4.16) was used as the limit-state function to determine the failure. A plot illustrating the probability of failure vs. time is plotted in Figure 4.6. And the probability of failure from SAEVSP and MCS are in Table 4.2.

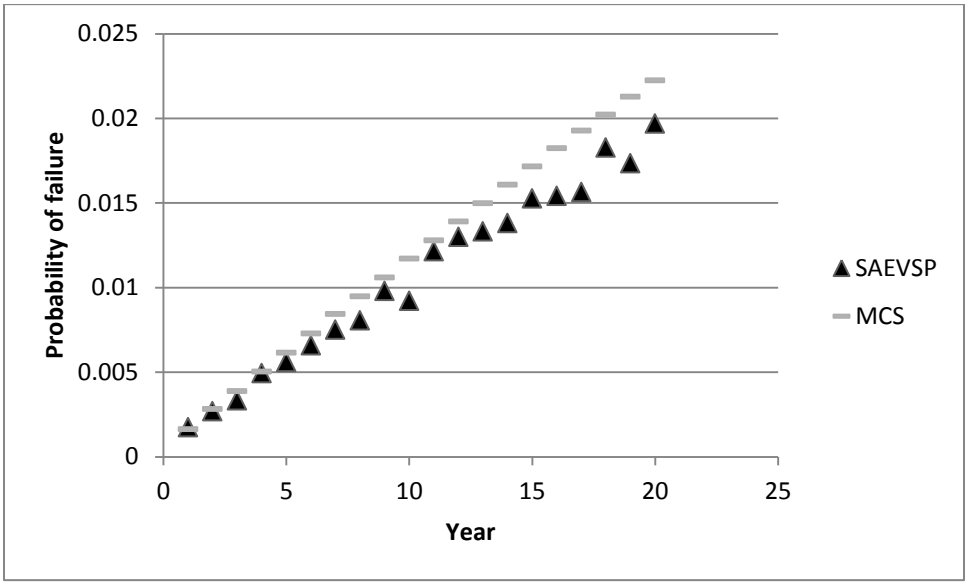

Figure 4.6. Probability of failure vs. time using limit-state 4.16 (d=0.033m)

Table 4.2. Probability of failure of deterministic design using Equation (4.16) with time

Time interval (Years)	SAEVSP	MCS
[0,1]	0.001731	0.001625
[0,2]	0.002677	0.00282
[0,3]	0.003322	0.003876
[0,4]	0.004937	0.005032
[0,5]	0.005601	0.006153
[0,6]	0.006579	0.007274
[0,7]	0.007517	0.008439
[0,8]	0.00805	0.009482
[0,9]	0.009803	0.010594
[0,10]	0.009203	0.011714
[0,11]	0.012149	0.012788
[0,12]	0.012998	0.013905
[0,13]	0.013318	0.014986
[0,14]	0.01381	0.016081
[0,15]	0.015261	0.017146
[0,16]	0.015418	0.018227
[0,17]	0.015638	0.019273
[0,18]	0.018275	0.020216
[0,19]	0.017343	0.02128
[0,20]	0.019691	0.022233

Similarly Equation (4.19) was used as the limit-state function to determine the failure. A plot illustrating the probability of failure vs. time is plotted in Figure 4.7. And the probability of failure from SAEVSP and MCS are in Table 4.3.

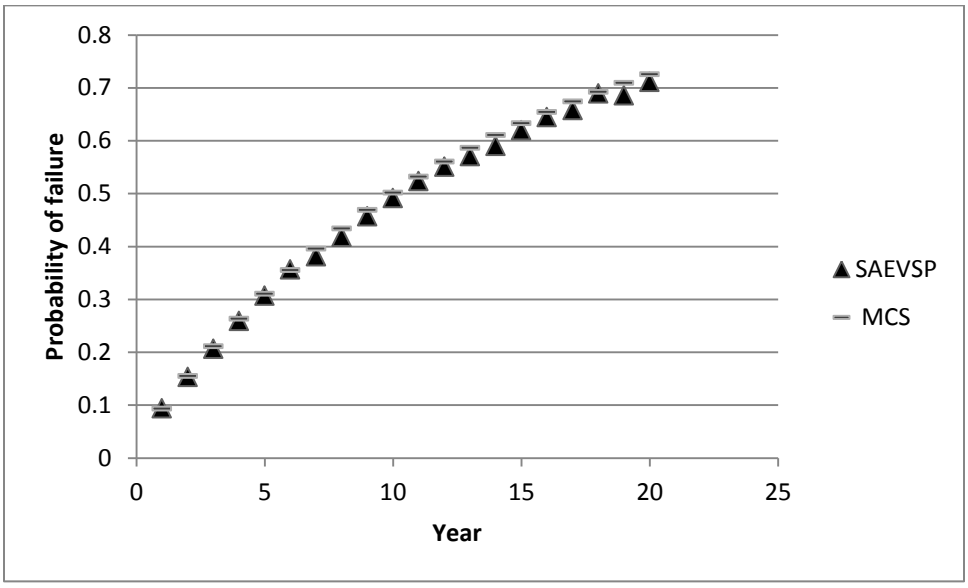

Figure 4.7. Probability of failure vs. time using limit-state 4.19 (d=0.033m)

Table 4.3. Probability of failure of deterministic design using Equation (4.19) with time

Time interval (Years)	SAEVSP	MCS
[0,1]	0.093972	0.093028
[0,2]	0.153292	0.154891
[0,3]	0.206469	0.211312
[0,4]	0.259209	0.263015
[0,5]	0.3068	0.310638
[0,6]	0.35621	0.354956
[0,7]	0.381551	0.395933
[0,8]	0.418082	0.433633
[0,9]	0.457145	0.468734
[0,10]	0.491308	0.501527
[0,11]	0.523699	0.53214
[0,12]	0.550474	0.56024
[0,13]	0.57081	0.586162
[0,14]	0.590047	0.610537
[0,15]	0.619481	0.633262
[0,16]	0.644202	0.654193
[0,17]	0.657974	0.673874
[0,18]	0.689005	0.692296
[0,19]	0.685849	0.709519
[0,20]	0.71107	0.725395

The results indicate that the probability of failure is high from failure due to the large deflection at section D of the shaft (Equation 4.19). Hence RBDO was performed using Equation (4.19) as limit-state with a required reliability of 0.99999. This implies that the probability of failure must be less than 0.00001 for the given time interval. Table 4.4 consists of the minimum shaft diameter based on RBDO. The diameter of the shaft is determined with respect to design life.

Table 4.4. RBDO results, optimum diameter with respect to design life

Time interval (Year)	Opt Diameter (m)
[0,1]	0.038803
[0,4]	0.039067
[0,8]	0.039114
[0,12]	0.039273
[0,16]	0.03932
[0,20]	0.039342

Now for a design life of 20 years, the shaft diameter from RBDO is 0.039342 m. For a conservative approach and considering manufacturing constraints, the diameter could be rounded to 0.04 m. Now reliability analysis was performed for 0.03934 m as the shaft diameter. The results from the SAEVSP are given in Table 4.5.

Table 4.5. Probability of failure for diameter from RBDO with time interval

Time interval (Years)	Probability of failure
[0,1]	0.0000016
[0,2]	0.0000022
[0,3]	0.0000014
[0,4]	0.0000046
[0,5]	0.0000037
[0,6]	0.0000028
[0,7]	0.0000053
[0,8]	0.0000043
[0,9]	0.0000085
[0,10]	0.0000017
[0,11]	0.0000100
[0,12]	0.0000094
[0,13]	0.0000099
[0,14]	0.0000082
[0,15]	0.0000098
[0,16]	0.0000081
[0,17]	0.0000066
[0,18]	0.0000112
[0,19]	0.0000084
[0,20]	0.0000108

4.6. DISCUSSIONS AND CONCLUSIONS

Foremost the probability of failure for a given time interval for deterministic design and reliability-based design were compared. The comparison is shown in Table 4.6. It can be clearly seen that the probability of failure from RBDO is much lower and is at acceptable level compared to that of the deterministic design. The increase in minimum diameter by using RBDO is 0.007m. This is 21% increase in the minimum shaft diameter from that of the deterministic design. For a time interval of 20 years, the probability of failure is brought down from 0.71107023 to 0.0000108 using RBD.

Table 4.6. Probability of failure comparison, deterministic design vs. reliability-based design

Time interval (Years)	Probability of failure	
	(D= 0.033 m)	(D= 0.03934 m)
[0,1]	0.09397182	0.0000016
[0,2]	0.15329229	0.0000022
[0,3]	0.20646911	0.0000014
[0,4]	0.25920900	0.0000046
[0,5]	0.30680022	0.0000037
[0,6]	0.35621047	0.0000028
[0,7]	0.38155094	0.0000053
[0,8]	0.41808151	0.0000043
[0,9]	0.45714529	0.0000085
[0,10]	0.49130777	0.0000017
[0,15]	0.61948083	0.0000098
[0,20]	0.71107023	0.0000108

Due to high computational cost using MCS, the rotor radius is considered as a deterministic design variable. This is because the BEM model needed to be run for each

sample of the radius would lead to high computational costs. By considering radius as a deterministic design variable the double iterative MCS process could be converted into a single iteration. The probability of failure using SAEVSP considering uncertainty in rotor radius was compared with reliability analysis in Table 4.7. The average percentage deviation from the actual probability of failure is 0.112%.

The average number of function calls for SAEVSP was 451 in comparison to that of 48000000 by MCS.

Table 4.7. Probability of failure with and without uncertainty in rotor radius for deterministic design

Time interval (Years)	Probability of failure		Percentage deviation
	Rotor radius deterministic	Rotor radius random variable	
[0,1]	0.093972	0.094276	0.323832
[0,2]	0.153292	0.153734	0.288117
[0,3]	0.206469	0.206925	0.221038
[0,4]	0.259209	0.259667	0.176775
[0,5]	0.3068	0.307231	0.140305
[0,6]	0.35621	0.356568	0.100411
[0,7]	0.381551	0.381865	0.082191
[0,8]	0.418082	0.418322	0.057574
[0,9]	0.457145	0.457278	0.029098
[0,10]	0.491308	0.491336	0.005749
[0,12]	0.550474	0.550293	0.032797
[0,14]	0.590047	0.589695	0.059508
[0,16]	0.644202	0.643585	0.095701
[0,18]	0.689005	0.688167	0.121749
[0,20]	0.71107	0.710153	0.128998

A relation is drawn of how the factor of safety used in deterministic design would compare with the minimum shaft diameter obtained from the reliability- based design.

This is illustrated in Figure 4.8. It can be seen that instead of the factor of safety of 1.5 used in the deterministic design, if a factor of safety of 2.5 was used, it would relate to using a reliability target of 0.99999 in RBDO.

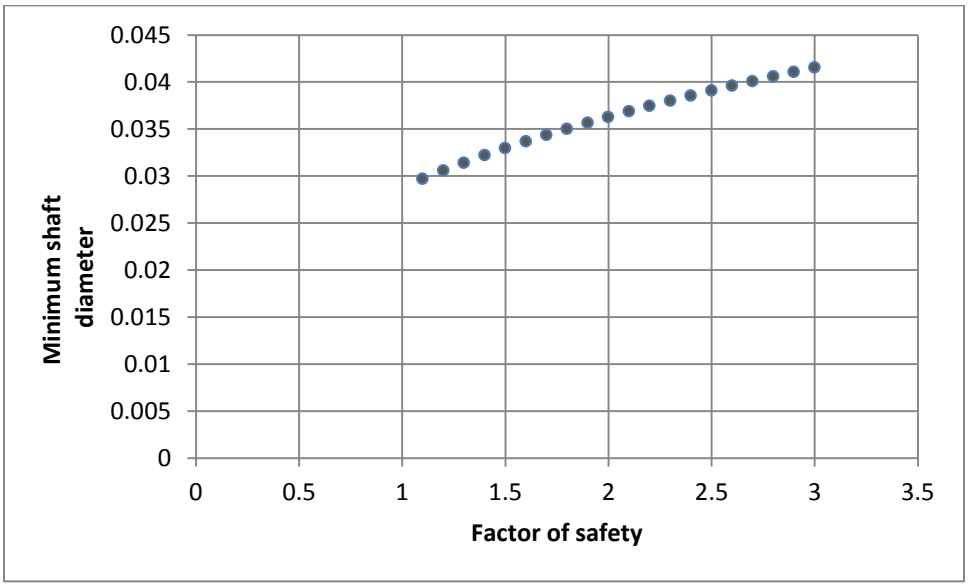

Figure 4.8. Minimum shaft diameter vs. factor of safety

5. CONCLUSIONS AND FUTURE WORK

5.1. CONCLUSIONS

Reliability is a major factor that needs to be considered during hydrokinetic system design. An efficient and reliable transmission shaft design methodology is presented for a design involving time variant uncertainty in the design parameters. In this work, we presented a model to determine the minimum transmission shaft diameter using both deterministic and reliability-based design.

The blade element momentum theory was used to evaluate the forces acting on the turbine blade and thus on the transmission shaft. All the possible modes of failure were assessed and a minimum shaft diameter was determined using deterministic design method. A reliability analysis was performed using the diameter obtained from deterministic design for a time interval of 20 years. The analysis showed that the probability of failure is unacceptable. Then a RBDO was performed to obtain the minimum shaft diameter taking considering all the uncertainties involved in the design. This yielded significantly higher reliability for a relatively small increase in the shaft diameter. The analysis also showed that the probability of failure is highly dependent on time. This is because of time-dependent stochastic process (river velocity) involved in the design. Use of the SAEVSP method was much more efficient compared to traditional MCS. This was because of the significantly lower number of evaluations of the limit-state function.

5.2. FUTURE WORK

Vertical river velocity profile was considered to be uniform while carrying out the design. This is true in case of small turbine rotor diameter such as the one discussed in the thesis. But in case of higher rotor diameters, this assumption may not stand true because the velocity profile could lead to an additional bending moment. Future work with this design could be to introduce the effect of vertical river velocity profile into the transmission shaft design model.

This design methodology could also be extended to the other components of the hydrokinetic turbine design for high reliability.

Additionally, it is seen from the results that the factor of safety in the deterministic design can be related to time-dependent reliability-based design. This could also be a potential area for further thought.

BIBLIOGRAPHY

[1] American Lung Association, "Toxic Air: The Case For Cleaning Up Coal-Fired Power Plants," American Lung Association, Washington, D.C, 2011.

[2] epa.gov, "Clean energy," [Online]. Available: http://www.epa.gov/cleanenergy/energy-and-you/affect/hydro.html. [Accessed 4 feb 2013].

[3] D. Hall, S. Cherry, K. Reeves, R. Lee, G. Carroll and G. Sommers, "Water energy resources of the united states with emphasis on low head/low power resources," U.S. Department of Energy, 2004.

[4] D. Hall, K. Reeves, J. Brizzee, R. Lee, G. Carroll and G. Sommers, "Wind and hydropower technologies, feasibility assessment of the water energy resources of the united states for new low power and small hydro classes of hydroelectric plants," Idaho National Laboratory, 2006.

[5] A. Date and A. Akbarzadeh, "Design and cost analysis of low head simple reaction hydro turbine for remote area power supply," *Renewable Energy,* vol. 409, no. 15, p. 34, 2009.

[6] M. Guney and K. Kaygusuz, "Hydrokinetic energy conversion systems: A technology status review," *Renewable and Sustainable Energy Reviews,* vol. 9, no. 14, pp. 2996-3004, 2010.

[7] R. Bedard, "Prioritized Research, Development, Deployment and Demonstration Needs: Marine and Other Hydrokinetic Renewable Energy," Electric Power Research Institute, 2008.

[8] M. Khan, M. Iqbal and J. Quaicoe, "River current energy conversion systems: Progress, prospects and challenges," *Renewable and Sustainable Energy Reviews,* vol. 2177, no. 93, p. 12, 2008.

[9] Office of Energy Efficiency and Renewable Energy, "Proceedings of the hydrokinetic and wave energy technologies technical and environmental issues workshop," U.S. Department of Energy:, Washington, D.C, 2006.

[10] M. Khan, G. Bhuyan, M. Iqbal and J. Quaicoe, "Hydrokinetic energy conversion systems and assessment of horizontal and vertical axis turbines for river and tidal applications: A technology status review," *Applied Energy,* vol. 86, no. 10, 1823-1835.

[11] Institute of Electrical and Electronics Engineers , *IEEE Standard Computer Dictionary: A Compilation of IEEE Standard Computer Glossaries.*, New York, 1990.

[12] A. Singh, Z. Mourelatos and E. and Nikolaidis, " Time-Dependent Reliability of Random Dynamic Systems Using Time-Series Modeling and Importance Sampling," *SAE International Journal of Materials and Manufacturing,* pp. 929-946, 2011.

[13] T. Cruse, Reliability based mechanical design, Marcel Dekker Inc., 1997.

[14] J. Tu, K. Choi and Y. Park, "A New Study on Reliability-Based Design Optimization," *Journal of Mechanical Design,* vol. 121, no. 4, 1999.

[15] X. Du and B. Huang, "Reliability Based Design Optimization with equality constraints," *International journal for numerical methods in engineering* , vol. 72, p. 1314:1331, 2007.

[16] X. Du, S. Agus and H. and Beiqing, "Reliability-Based Design with the Mixture of Random and Interval Variables," *Journal of Mechanical Design,* vol. 127, no. 6, pp. 1068-1076, 2005.

[17] G. A. Hazelrigg, "A Framework for Decision-Based Engineering Design," *Journal of Mechanical Design,* vol. 120, pp. 653-658, 1998.

[18] C. L. Dym and P. Little, Engineering Design, New York: Wiley, 2004.

[19] G. J. Klir and M. J. Wierman, Uncertainty Based Information : Elements of Generalized Information Theory, Physica-Verlag, 1998.

[20] M. O. Hansen, Aerodynamics of wing turbine, Sterling, VA: Earthscan, 2008.

[21] J. E. Shigley, C. R. Mischke and R. G. Budynas, "Shafts and Axles," in *Mechanical Engineering Design*, The McGraw-Hills Companies, 2004.

[22] N. L.Pedrsen, "Optimization of Keyway Design," in *2nd International Conference on Engineering Optimization*, Lisbon, Portugal, 2010.

[23] V. N and S. Danny, "Flow chardacteristics of river resourses for hydrokinetic energy conversion," in *Hydrovision International*, Charlotte, NC, 2010.

[24] Z. Hu and X. Du, "Time-Dependent Reliability Analysis by a Sampling approach to extreme values of stochastic processes," in *International Design Engineering Technical Conferences and Computers and information in Engineering Conference*, Chicago, IL, 2012.

[25] L. Leopold, "Downstream change of velocity in river," *American Journal of Science*, 1953.

[26] V. Arora and G. Boer, "A variable velocity flow routing algoritm for GCMs," *Journal of Geophysical Research*, p. 104, 1999.

[27] H. Schulze, M. Hunger and P. Doll, "Simulating river flow velocity on global scale," *Advances in Geosciences*, 2005.

[28] P. Allen, J. Arnold and B. Byars, "Downstream channel geometry for use in planning-level models," *Water Resources Bulletin*, 1994.

[29] L. Leopold and T. Maddock, "The hydraulic geometry of stream channels and some physiographic implications," *United States Geological Survey,* 1953.

[30] J. Beersma and T. Buishand, "Joint probability of precipitation and discharge deficits in Nethearlands," *Water Resourses Research*, 2004.

[31] H. Mitosek, "On stochastic properties of daily river flow processes," *Journal of Hydrology*, 2000.

[32] Database RD. Gaylord Nelson institute of environmental studies, [Online]. Available: http://www.sage.wisc.edu/riverdata/scripts/station_table.php?qual=32&filenum=1457. [Accessed 12 January 2013].

[33] J. M. Van Noortwijk, J. a. M. Van Der Weide, M. J. Kallen and M. D. and Pandey, "Gamma Processes and Peaks-over-Threshold Distributions for Time-Dependent Reliability," *Reliability Engineering and System Safety*, pp. 1651-1658, 2007.

[34] G. Tont, L. Vlădăreanu, M. S. Munteanu and D. G. and Tont, " Markov Approach of Adaptive Task Assignment for Robotic System in Non-Stationary Environments," *WSEAS Transactions on Systems,* pp. 273-282, 2010.

[35] L. D. Lutes and S. And Sarkani, "Reliability Analysis of Systems Subject to First-Passage Failure," 2009.

[36] B. Sudret, "Analytical Derivation of the Outcrossing Rate in Time-Variant Reliability Problems," *Structure and Infrastructure Engineering,* pp. 353-362, 2008.

[37] P. H. Madsen and S. and Krenk, "Integral Equation Method for the First-Passage Problem in Random Vibration," *Journal of Applied Mechanics, Transactions ASME,* vol. 51, no. 3, pp. 674-679, 1984.

[38] Brook Tech, "General Dimentional Tolerance," Brook Tech, [Online]. Available: http://www.brook-tech.fsnet.co.uk/reference.htm. [Accessed 21 January 2013].

[39] K. Nair, "Pico-Spiral-Wind-Turbine," 31 March 2013. [Online]. Available: http://www.behance.net/gallery/Pico-Spiral-Wind-Turbine/1709919.

VITA

Goutham Pusapati was born on November 8, 1988, in Visakhapatnam, India. He did his initial schooling at Sainik School Korukonda and later at Srichaitanya Junior College, Visakhapatnam, India. He received his Bachelor of Engineering degree with distinction in Mechanical Engineering from Andhra University, Visakhapatnam in 2010. He then pursued his Master of Science in Mechanical Engineering at Missouri University of Science and Technology, Rolla, MO and graduated in May 2013.